

# PCA recovery thresholds in low-rank matrix inference with sparse noise

Urte Adomaityte\*, Gabriele Sicuro†, Pierpaolo Vivo\*

\*King's College London, Department of Mathematics, Strand, London WC2R 2LS, United Kingdom

†University of Bologna, Department of Mathematics,  
Piazza di Porta San Donato 5, 40126, Bologna, Italy

We study the high-dimensional inference of a rank-one signal corrupted by sparse noise. The noise is modelled as the adjacency matrix of a weighted undirected graph with finite average connectivity in the large size limit. Using the replica method from statistical physics, we analytically compute the typical value of the top eigenvalue, the top eigenvector component density, and the overlap between the signal vector and the top eigenvector. The solution is given in terms of recursive distributional equations for auxiliary probability density functions which can be efficiently solved using a population dynamics algorithm. Specialising the noise matrix to Poissonian and Random Regular degree distributions, the critical signal strength is analytically identified at which a transition happens for the recovery of the signal via the top eigenvector, thus generalising the celebrated BBP transition to the sparse noise case. In the large-connectivity limit, known results for dense noise are recovered. Analytical results are in agreement with numerical diagonalisation of large matrices.

## I. INTRODUCTION

The estimation of a low-rank signal from a noisy observation in high dimensions is a fundamental problem in machine learning, statistics and probability. This task appears in Principal Component Analysis (PCA) [1, 2], community detection [3, 4] or matrix completion [5], among others. Spiked random matrix models have been extensively investigated as a prototypical setup for the theoretical modelling of these problems [6–8]. In the rank-one signal case, one seeks to recover a vector  $x \in \mathbb{R}^N$  from a noisy observation

$$\mathbf{A} = \mathbf{J} + \frac{\theta}{N} xx^\top, \quad (1)$$

where  $\theta$  is the signal-to-noise ratio and the noise is modelled via the random matrix  $\mathbf{J} \in \mathbb{R}^{N \times N}$ , typically dense, full-rank and random. For various assumptions on the spike and noise matrix, observables of interest that quantify signal recovery are the value of the typical top eigenvalue, the overlap of the top eigenvector with the signal, the spectral density, and the top eigenvalue distribution. Of special interest are BBP-like transitions in the signal strength (named after the authors of Ref. [7]): a value  $\theta_{\text{crit}}$  such that for  $\theta > \theta_{\text{crit}}$  the top eigenvalue detaches from the right bulk edge of the spectrum, the top eigenvector aligns non-trivially with the signal, and a naïve spectral algorithm succeeds in recovering the signal. We illustrate this mechanism in Fig. 1.

In this work, we analyse the recovery threshold of naïve PCA, that is, recovery of the signal via the top eigenvector of the matrix  $\mathbf{A}$  when the assumption that the noise  $\mathbf{J}$  is dense is dropped. There is a wealth of important applications in which the *sparse* structure of the noise [12] is relevant, such as video, image, multimedia processing, notably video surveillance and facial recognition (see [2, 13] for more detailed accounts), yet the classical random matrix toolkit is ineffective when one cannot rely on rotational invariance and Gaussian assumptions on the matrix entries. Borrowing tools from the physics

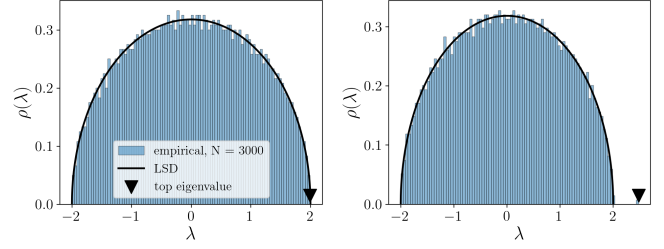


FIG. 1. The BBP-like transition for the matrix model Eq. (1), where  $\mathbf{J}$  is a (dense) GOE matrix constructed as  $\mathbf{J} = (\mathbf{G} + \mathbf{G}^\top)/\sqrt{2N}$  with  $G_{ij} \stackrel{\text{i.i.d.}}{\sim} \mathcal{N}(0, 1)$  and spike components  $x_i \stackrel{\text{i.i.d.}}{\sim} \mathcal{N}(0, 1)$ . In this case, the recovery threshold is known to be  $\theta_{\text{crit}} = 1$  [9–11]. Left: for signal strength  $\theta \leq \theta_{\text{crit}}$ , as  $N \rightarrow \infty$ , the top eigenvalue of  $\mathbf{A}$  sits at the right edge of the limiting spectral density (LSD)  $\varrho(\lambda) = \frac{1}{2\pi} \sqrt{4 - \lambda^2}$ ,  $\lambda \in [-2, 2]$  of  $\mathbf{J}$ . Right: for  $\theta > \theta_{\text{crit}}$ , the top eigenvalue of  $\mathbf{A}$  is an outlier at  $\lambda_{\text{top}} = \theta + \frac{1}{\theta}$  [9–11]. The histogram represents the spectrum of a size  $N = 3 \times 10^3$  matrix for  $\theta = 0$  (left) and  $\theta = 2$  (right).

of disordered systems, we have been able to overcome this technical challenge and present analytical results for important spectral observables in the *sparse spiked problem*, including a precise characterisation of the recovery threshold that generalises the celebrated BBP transition to the sparse noise case.

We employ the replica formalism [14] developed by [15–17] and used in [18–21] to calculate spectral properties of large symmetric matrices with sparse structure, namely when the average connectivity of the noise matrix remains finite as  $N \rightarrow \infty$ . The extremal observables are determined via the solution of coupled recursive distributional equations (RDEs), i.e., integral equations for auxiliary probability density functions, which can be efficiently solved using a population dynamics algorithm [22]. RDEs appear in statistical physics and inference [23, 24] in the analysis of infinite-graph-size solutions

of message-passing/belief propagation algorithms. They are recovered in the mathematical literature as ‘stochastic recursive equations’ in problems on random graphs; see [25–28] for their analysis of the Google PageRank vector distribution. Other network centrality measures are analysed via the cavity formalism that leads to RDEs solved via population dynamics in [29]. The cavity method, exact for sparse tree structures [30], is also used as an alternative to the replica calculation and leads to the same results for the spectral density [31], top and second eigenpair problems [19, 20].

For a model like Eq. (1) but with a sparse  $\mathbf{J}$  (see Section II), we obtain the value of the typical top eigenvalue, the density of the components of the top eigenvector, the typical value of the overlap between the spike vector and the top eigenvector and the density of its components. We also compute the threshold value  $\theta_{\text{crit}}$  at which the top eigenvector starts to correlate with the spike, i.e., the overlap becomes non-trivial. This depends on the structural parameters of the spiked matrix model  $\mathbf{A}$  such as the average connectivity and assumptions on the bond weight and spike component distributions. We further show that in the large connectivity limit, we recover known values of the BBP-like transition, the top eigenvalue and the squared overlap for the spiked real Wigner matrix ensemble [9–11].

In the next section, we review the related literature in inference, statistical physics and machine learning.

### A. Related works

The analysis of detection limits in large spiked random matrix models, where the noise is assumed to be a large random matrix that is added to the low-rank signal matrix, began with works on phase transitions in the spiked Wishart [7] and spiked Wigner [9–11] models. An earlier seminal work [6] employs random matrix theory to analyse the distribution of the top eigenvalue of a large covariance matrix model, motivated by the analysis of PCA. It has inspired a wide array of works in multiple domains, with a particular focus on high-dimensional limits, e.g., [32–35]. Ref. [36] considers the top eigenvalue and squared overlap of the case where either the noise matrix or the signal is rotationally (or unitarily) invariant. Large deviations of the top eigenvalues have also been considered for dense random matrices with a rank-one spike [37].

Our paper aims to determine the extent to which naively applying PCA affects the recovery of the low-rank signal in high dimensions, if one is agnostic to the sparsity of the noise. Once it is known that the noise structure is sparse, there is an array of specialised PCA algorithms one can apply, namely Robust PCA [2, 38] to recover the low-rank matrix  $L$  and the sparse noise matrix  $S$  from an observation  $L + S$ . Notable extensions include [13, 39–43]. For a dense noise model, universality of the Fisher information in recovery was established in

terms of the minimum mean squared error (MMSE) in [44], where a dense probabilistic analogue of the sparse noise matrix is covered: small noise is added with probability  $p$  and large noise with probability  $1 - p$ .

There is a current line of works that generalises assumptions on the noise matrix  $\mathbf{J}$  in low-rank matrix inference to analyse algorithmic recovery thresholds, albeit in the case where  $\mathbf{J}$  remains dense. In particular, known BBP-like transition values and efficient algorithms that incorporate prior information such as Approximate Message Passing (AMP) are derived that perform well where naïve spectral methods such as PCA would fail. In particular, Ref. [45] considers heterogeneous but dense noise, prove Gaussian universality of the free energy and the spectrum and determine an information theoretical threshold for the dense degree-corrected Stochastic Block Model. Refs. [46–49] consider dense block-structured noise models, while Ref. [50] analyses non-linear observation channels with zero Fisher information and provides a unified view of theoretical thresholds and optimal AMP algorithms for that class of models. Also, Ref. [51] considers rotationally invariant dense noise and evaluate how Bayes estimators and AMP perform with mismatched noise priors (incorrectly assuming Gaussian noise in particular), while Refs. [52, 53] extend AMP for a spiked model where dense noise is no longer independent but still rotationally invariant, and provide information-theoretical limits along with an efficient algorithm. Note, however, that contrary to our setup, they consider dense noise matrices and determine algorithmic thresholds.

Spectral algorithms on a sparse matrix are studied in community detection tasks, where [54] first studied the non-backtracking operator (introduced in [55] in the context of zeta functions): unlike working with the adjacency matrix, spectral algorithms on this operator achieve information-theoretical performance; its spectral properties are investigated further in [56, 57]. The cavity method is also employed in community detection on sparse adjacency matrices with finite connectivity, see [58] and references therein. The non-backtracking operator is also studied in the top eigenpair problem for (unspiked) sparse matrices via the cavity method in [17, 19]. Recently, [59] analysed the top eigenvalue detection via the real-valued cavity method for the Anderson model [60] and found that criteria for finding the solution based on the non-backtracking operator are unsatisfactory when the top eigenvector is localised. Localisation transitions of sparse graph adjacency matrices are studied in [61, 62], and a treatment of the case of sparse non-Hermitian matrices is in [63, 64].

More broadly, the structure of ‘sparse plus low-rank’ large size matrices appears in recent works on fine-tuning and compression methods for large language models, motivated by the considerable storage and training costs incurred because of their size. In Ref. [65], the authors improve the memory efficiency of the industry-standard fine-tuning technique low-rank adaptation (LoRA) [66], where a dense pre-trained weight matrix is updated with

a low-rank correction, by parametrising the dense weight matrix as a sparse plus low rank structure. Additionally, the ‘sparse plus low-rank’ matrix structure is key in Ref. [67]: an outlier-aware thresholding method (akin to Robust PCA) used to compress LLMs by decomposing the weight matrices into a sum of a sparse matrix and a low-rank matrix; it achieves significant speed-up on inference without retraining and state-of-the-art performance on some benchmarks.

## B. Outline

The presentation of the model and the formulation of the optimisation problem in terms of replica analysis is provided in Section II. The main results are outlined in Section III and specialised in Section IV to particular degree distributions. We conclude and present an outlook for future works in Section V. The Appendices are devoted to the full replica calculations, technical derivations and the description of the population dynamics algorithm.

## II. THE MODEL

We will consider a  $N \times N$  symmetric random matrix in the form

$$\mathbf{A} = \mathbf{C} \odot \mathbf{W} + \frac{\theta}{N} \mathbf{x} \mathbf{x}^\top, \quad (2)$$

where  $\odot$  is the Hadamard product multiplying two  $N \times N$  matrices element-wise.

The *signal*  $\mathbf{x} \in \mathbb{R}^N$  is constructed by sampling identically and independently each of its components  $x_i$  from a density  $\varrho_x$  on  $\mathbb{R}$ . We will work with distributions with zero mean and finite second moment. The parameter  $\theta \geq 0$  modulates the strength of the rank-one “spike”  $\mathbf{x} \mathbf{x}^\top$ .

Both the matrix  $\mathbf{C} = (c_{ij})_{ij} \in \{0, 1\}^{N \times N}$  and the matrix  $\mathbf{W} = (W_{ij})_{ij} \in \mathbb{R}^{N \times N}$  are assumed to be symmetric and random, so that  $\mathbf{J} := \mathbf{C} \odot \mathbf{W}$  plays the role of a *symmetric noise matrix*. The matrix  $\mathbf{J}$  is sparse; its average connectivity remains finite as the size  $N \rightarrow \infty$ . To be more precise, we construct  $\mathbf{C}$  by considering the adjacency matrix of an undirected random graph of  $N$  vertices sampled from the configuration model ensemble, with degree sequence  $k := (k_1, \dots, k_N)$ . The degree  $k_i$  of the  $i$ th node is independently sampled from a distribution  $p_k$ , identically for all vertices. The distribution  $p_k$  is assumed to have finite support with largest element  $k_{\max}$ . Given a function  $f$  defined on the support of  $p_k$ , we will use the notation

$$\langle f(k) \rangle := \sum_k f(k) p_k.$$

In particular, we will denote

$$c := \langle k \rangle$$

the average degree of the vertices in the auxiliary graph.

We will therefore assume the joint distribution of entries of  $\mathbf{J}$  to be in the form

$$P(\mathbf{J}|k) = P(\mathbf{C}|k) p(\mathbf{W}) \prod_{ij} \delta(J_{ij} - c_{ij} W_{ij}). \quad (3)$$

The distribution of connectivities given the degree sequence has the form

$$P(\mathbf{C}|k) \propto \prod_{i=1}^N \delta_{c_{ii}, 0} \mathbb{I} \left( \sum_{j=1}^N c_{ij} = k_i \right) \quad (4)$$

where  $\mathbb{I}(S) = 1$  if  $S$  is true and 0 otherwise. The density of bond weights is assumed to be in the form

$$p(\mathbf{W}) = \prod_{i < j} \delta(W_{ij} - W_{ji}) \varrho_W(W_{ij}) \prod_i \delta(W_{ii}), \quad (5)$$

where the density  $\varrho_W$  has a compact support with upper edge  $\zeta$  and  $\mathbb{E}_W[W] \neq 0$ . The Gershgorin circle theorem [68] implies then that the top eigenvalue  $\lambda_{\text{top}}$  of  $\mathbf{A}$  is of  $\mathcal{O}(1)$  for large  $N$ . For illustration, we will consider two special cases specified by the choice of  $p_k$ :

**Poisson:** In the Poissonian connectivity setup, the distribution  $p_k$  is assumed to be a *truncated* Poisson distribution depending on the parameter  $\bar{c} > 0$

$$p_k = \frac{\bar{c}^k}{\Gamma k!}, \quad \Gamma := \sum_{k=0}^{k_{\max}} \frac{\bar{c}^k}{k!}, \quad k \in \{0, 1, \dots, k_{\max}\}, \quad (6)$$

where the relation between  $c$  and  $\bar{c}$  is given by  $c := \langle k \rangle = \sum_{k=0}^{k_{\max}} k \frac{\bar{c}^k}{k!} / \sum_{k=0}^{k_{\max}} \frac{\bar{c}^k}{k!}$ . In this distribution, the expected average degree  $c = \langle k \rangle \rightarrow \bar{c}$  as  $k_{\max} \rightarrow +\infty$ .

**Random regular:** In the random regular (RR) setup, we simply pick

$$p_k = \delta_{k, c} \quad (7)$$

for a certain  $c = k_{\max} > 1$ .

Recall however that the results we obtain are valid for general  $p_k$  satisfying the assumptions.

### A. The top eigenvalue

We will now sketch the main ideas behind the replica calculation to characterise the statistical properties of the typical top eigenvalue  $\lambda_{\text{top}}$  of  $\mathbf{A}$ . We will see, in particular, that the *replica trick* is a powerful tool to study a variety of relevant observables in the large  $N$  limit.

Let us start by observing that, by means of the Courant–Fischer–Weyl min–max principle, it is possible to characterise the top eigenvalue  $\lambda_{\text{top}}$  of  $\mathbf{A}$  as

$$N \lambda_{\text{top}} = \max_{\|\mathbf{v}\|^2=N} \langle \mathbf{v}, \mathbf{A} \mathbf{v} \rangle,$$

where  $\langle \cdot, \cdot \rangle$  is the dot product between vectors in  $\mathbb{R}^N$ . Under a non-degeneracy assumption, the maximum is achieved by a single vector  $v_{\text{top}}$  (up to a  $\mathbb{Z}_2$  symmetry), corresponding to the eigenvector associated to  $\lambda_{\text{top}}$ . This fact suggests that we may recast the problem into a quadratic optimisation problem, namely introduce the Gibbs-Boltzmann distribution in the form

$$P_\beta(v; \mathbf{A}) = \frac{1}{Z_\beta(\mathbf{A})} \exp\left(\frac{\beta}{2} \langle v, \mathbf{A}v \rangle\right) \delta(\|v\|^2 - N), \quad (8)$$

with the partition function

$$Z_\beta(\mathbf{A}) := \int dv \exp\left(\frac{\beta}{2} \langle v, \mathbf{A}v \rangle\right) \delta(\|v\|^2 - N). \quad (9)$$

By means of a saddle-point approach in the  $N \rightarrow \infty$  limit, the solution is obtained in the low temperature limit  $\beta \rightarrow \infty$  as the measure concentrates on the eigenvector associated to the top eigenvalue. As a consequence,

$$\mathbb{E}_\mathbf{A}[\lambda_{\text{top}}] = \lim_{N \rightarrow \infty} \lim_{\beta \rightarrow \infty} \frac{2}{\beta N} \mathbb{E}_\mathbf{A}[\ln Z_\beta(\mathbf{A})]. \quad (10)$$

Taking the average of the logarithm of the partition function is famously cumbersome, so we employ the celebrated replica trick [14] to write

$$\mathbb{E}_\mathbf{A}[\lambda_{\text{top}}] = \lim_{N \rightarrow \infty} \lim_{\beta \rightarrow \infty} \frac{2}{\beta N} \lim_{n \rightarrow 0} \frac{1}{n} \ln \mathbb{E}_\mathbf{A}[Z_\beta^n(\mathbf{A})]. \quad (11)$$

The bulk of the technical part is dedicated to computing  $\mathbb{E}_\mathbf{A}[Z_\beta^n(\mathbf{A})]$ , the average of the partition function replicated  $n$  times, where  $n$  is first taken as an integer and then analytically continued to real values around  $n = 0$ . Note that in practice, there is an implicit assumption that the limit  $N \rightarrow \infty$  and the replica limit  $n \rightarrow 0$  can be exchanged to give

$$\mathbb{E}_\mathbf{A}[\lambda_{\text{top}}] = \lim_{\beta \rightarrow \infty} \frac{2}{\beta} \lim_{n \rightarrow 0} \frac{1}{n} \lim_{N \rightarrow \infty} \frac{1}{N} \ln \mathbb{E}_\mathbf{A}[Z_\beta^n(\mathbf{A})]. \quad (12)$$

The full calculation is presented in Appendix A.

## B. Eigenvector of the top eigenvalue

Let us show now how some properties of the eigenvector associated to  $\lambda_{\text{top}}$  can be computed via the same trick. Suppose that we are given a function  $F: \mathbb{R} \times \mathbb{R}^N \times \mathbb{R}^N \rightarrow \mathbb{R}$ . Let  $x$  be the spike vector as defined by the model formulation and  $v_{\text{top}}$  the eigenvector of  $\mathbf{A}$  corresponding to  $\lambda_{\text{top}}$ , hereafter also referred to as *top eigenvector*. Suppose that we are interested in the calculation of  $\lim_N \mathbb{E}_\mathbf{A}[F(u, v_{\text{top}}, x)]$ . A strategy is to consider the following auxiliary partition function [19]

$$Z_\beta[\mathbf{A}; tF] :=$$

$$= \int dv \exp\left[\frac{\beta}{2} \langle v, \mathbf{A}v \rangle + \beta t N F(u, v, x)\right] \delta(\|v\|^2 - N), \quad (13)$$

and compute the quantity of interest as

$$\begin{aligned} & \lim_{N \rightarrow +\infty} \mathbb{E}_\mathbf{A}[F(u, v_{\text{top}}, x)] \\ &= \lim_{N \rightarrow +\infty} \lim_{\beta \rightarrow +\infty} \frac{1}{\beta N} \frac{\partial}{\partial t} \mathbb{E}_\mathbf{A}[\ln Z_\beta[\mathbf{A}; tF]] \Big|_{t=0} \\ &= \lim_{\beta \rightarrow +\infty} \lim_{n \rightarrow 0} \lim_{N \rightarrow +\infty} \frac{1}{n \beta N} \frac{\partial}{\partial t} \ln \mathbb{E}_\mathbf{A}[(Z_\beta[\mathbf{A}; tF])^n] \Big|_{t=0}, \end{aligned} \quad (14)$$

where in the last line a replicated partition function appears and we assume again that one can exchange the limits  $n \rightarrow 0$  and  $N \rightarrow \infty$ . We remark that the partition function  $Z_\beta(\mathbf{A})$  in Eq. (9) follows from setting  $t = 0$  in Eq. (13).

This simple observation allows us to access a series of relevant observables. For example, we are interested in the asymptotic *density of the entries of the top eigenvector*  $v_{\text{top}}$

$$\varrho_{\text{top}}(u) = \mathbb{E}_\mathbf{A} \left[ \frac{1}{N} \sum_{i=1}^N \delta(u - v_{\text{top},i}) \right]. \quad (15)$$

This quantity can be computed via the aforementioned strategy by choosing for  $F$  in Eq. (14) the function

$$F(u, v, x) \mapsto F_{\text{top}}(u, v) := \frac{1}{N} \sum_{i=1}^N \delta(u - v_i).$$

Similarly, it is possible to compute the average *overlap* between  $v_{\text{top}}$  and the spike  $x$ , by estimating first the density

$$\varrho_{\text{ov}}(u) \mathbb{E}_\mathbf{A} \left[ \frac{1}{N} \sum_{i=1}^N \delta(u - x_i v_{\text{top},i}) \right], \quad (16)$$

with the choice

$$F(u, v, x) \mapsto F_{\text{ov}}(u, v, x) := \frac{1}{N} \sum_{i=1}^N \delta(u - x_i v_i),$$

and then computing

$$\lim_{N \rightarrow \infty} \mathbb{E}_\mathbf{A} \left[ \frac{\langle x, v_{\text{top}} \rangle}{N} \right] = \lim_{N \rightarrow \infty} \int u \varrho_{\text{ov}}(u) du. \quad (17)$$

## III. MAIN RESULTS

The discussion in Section II A showed that the knowledge of the average replicated partition function provides a significant amount of information on a series of relevant observables. We present the full calculation in Appendix A of a series of crucial quantities. In this section we will summarise the main results.

Before proceeding, let us introduce a convenient auxiliary quantity and notation. Let  $p_k$  be the degree distribution of the configuration model with truncated largest degree  $k_{\max}$ . We will denote

$$r_k := \frac{kp_k}{c}, \quad k \in \{1, \dots, k_{\max}\} \quad (18)$$

the associated *degree-corrected degree distribution*. In the following, given a function  $f$  defined on the positive integers, we will denote

$$\langle\langle f(k) \rangle\rangle := \sum_{k=1}^{k_{\max}} r_k f(k).$$

Moreover, in the following, we will use the shorthand notation  $\{d\mu\}_s := \prod_{\ell=1}^s \mu(z_\ell) dz_\ell$  for a given density  $\mu(z)$  on a domain of  $\mathbb{R}^d$ , and the notation  $\{u\}_s := \sum_{\ell=1}^s u_\ell$  for an indexed collection of scalar variables.

**Result III.1** (Self-consistent equations and top eigenvalue). *Let  $X \sim \varrho_x$  be a random variable. Let  $\pi(\omega, h)$  be the joint probability density of the pair  $(\omega, h)$  with  $\omega > 0$ , solution of the following recursive distributional equation*

$$\begin{aligned} \pi(\omega, h) = \mathbb{E}_X \left\langle \int \{d\pi\}_{k-1} \{d\varrho_W\}_{k-1} \right. \\ \left. \times \delta \left( \omega - \lambda_\theta + \left\{ \frac{W^2}{\omega} \right\}_{k-1} \right) \delta \left( h - \left\{ \frac{hW}{\omega} \right\}_{k-1} - \theta q X \right) \right\rangle, \end{aligned} \quad (19a)$$

supplemented with the following conditions that fix the parameters  $\lambda_\theta$  and  $q$

$$1 = \mathbb{E}_X \left\langle \int \{d\pi\}_k \{d\varrho_W\}_k \left( \frac{\left\{ \frac{hW}{\omega} \right\}_k + \theta q X}{\lambda_\theta - \left\{ \frac{W^2}{\omega} \right\}_k} \right)^2 \right\rangle, \quad (19b)$$

$$q = \mathbb{E}_X \left\langle \int \{d\pi\}_k \{d\varrho_W\}_k \frac{X \left\{ \frac{hW}{\omega} \right\}_k + \theta q X^2}{\lambda_\theta - \left\{ \frac{W^2}{\omega} \right\}_k} \right\rangle. \quad (19c)$$

Then the average top eigenvalue  $\lambda_{\text{top}}$  of the matrix  $\mathbf{A}$  is equal to the parameter  $\lambda_\theta$  satisfying Eqs. (19), namely

$$\mathbb{E}_{\mathbf{A}}[\lambda_{\text{top}}] = \lambda_\theta. \quad (20)$$

The numerical solution  $\pi(\omega, h)$  of Eqs. (19) can be efficiently obtained using a population dynamics algorithm, as described in Appendix C. The knowledge of  $\pi(\omega, h)$  satisfying Eqs. (19) allows us to compute the top eigenvector properties in Eqs. (15) and (16).

**Result III.2** (Typical density of the top eigenvector components). *The following holds*

$$\begin{aligned} \varrho_{\text{top}}(u) = \\ = \mathbb{E}_X \left\langle \int \{d\pi\}_k \{d\varrho_W\}_k \delta \left( u - \frac{\left\{ \frac{hW}{\omega} \right\}_k + \theta q X}{\lambda_\theta - \left\{ \frac{W^2}{\omega} \right\}_k} \right) \right\rangle. \end{aligned} \quad (21)$$

**Result III.3** (Typical density of the overlap components). *The typical overlap density is given by*

$$\begin{aligned} \varrho_{\text{ov}}(u) = \\ = \mathbb{E}_X \left\langle \int \{d\pi\}_k \{d\varrho_W\}_k \delta \left( u - \frac{X \left\{ \frac{hW}{\omega} \right\}_k + \theta q X^2}{\lambda_\theta - \left\{ \frac{W^2}{\omega} \right\}_k} \right) \right\rangle. \end{aligned} \quad (22)$$

**Remark III.1** (Degree decomposition). Observe that the density of the top eigenvector components and of the overlap between the top eigenvector and the signal in Eqs. (21) and (22) are naturally decomposed as superpositions of contributions coming from nodes of different degrees (see Fig. 5 for explicit examples of such node decomposition).

Using  $\varrho_{\text{ov}}(u)$  from Eq. (22), we easily obtain the average value of the overlap and squared overlap between the top eigenvector and the signal.

**Result III.4** (Overlap and squared overlap). *The overlap and squared overlap between the top eigenvector and the signal are given by*

$$\begin{aligned} \mathbb{E}_{\mathbf{A}} \left[ \frac{\langle x, v_{\text{top}} \rangle}{N} \right] = \int du \varrho_{\text{ov}}(u) u = \\ = \mathbb{E}_X \left\langle \int \{d\pi\}_k \{d\varrho_W\}_k \frac{X \left\{ \frac{hW}{\omega} \right\}_k + \theta q X^2}{\lambda_\theta - \left\{ \frac{W^2}{\omega} \right\}_k} \right\rangle \end{aligned} \quad (23)$$

and

$$\begin{aligned} \mathbb{E}_{\mathbf{A}} \left[ \frac{\langle x, v_{\text{top}} \rangle^2}{N^2} \right] = \int du \varrho_{\text{ov}}(u) u^2 = \\ = \mathbb{E}_X \left\langle \int \{d\pi\}_k \{d\varrho_W\}_k \left( \frac{X \left\{ \frac{hW}{\omega} \right\}_k + \theta q X^2}{\lambda_\theta - \left\{ \frac{W^2}{\omega} \right\}_k} \right)^2 \right\rangle, \end{aligned} \quad (24)$$

respectively.

**Remark III.2** (Interpretation of  $q$ ). Note that, in light of Eq. (23), Eq. (19c) implies that  $q$  can be interpreted as the average overlap between the top eigenvector and the signal.

**Remark III.3** (Reduction to the pure noise matrix). Setting  $\theta = 0$  or  $\varrho_x(x) = \delta(x)$  the spike in Eq. (2) is removed and the results in Eq. (19a), (19b) and (21) recover the properties of the top eigenpair of sparse graphs derived in [19], as expected.

To conclude, we state the results for the critical value  $\theta_{\text{crit}}$  for a general degree distribution  $p_k$ . Let us assume that the spike is sampled from a distribution such that  $\mathbb{E}_X[X] = 0$  and  $\sigma_x^2 := \mathbb{E}_X[X^2]$  finite. The critical value  $\theta_{\text{crit}}$  is such that for  $\theta \leq \theta_{\text{crit}}$  we have  $\mathbb{E}_{\mathbf{A}}[\lambda_{\text{top}}] = \lambda_{\theta=0}$  (average top eigenvalue in absence of a signal), and the average overlap between the signal and the top eigenvector  $\mathbb{E}_{\mathbf{A}}[\frac{1}{N} \langle x, v_{\text{top}} \rangle] = 0$ , indicating that the signal cannot be recovered by looking at the top eigenvector.

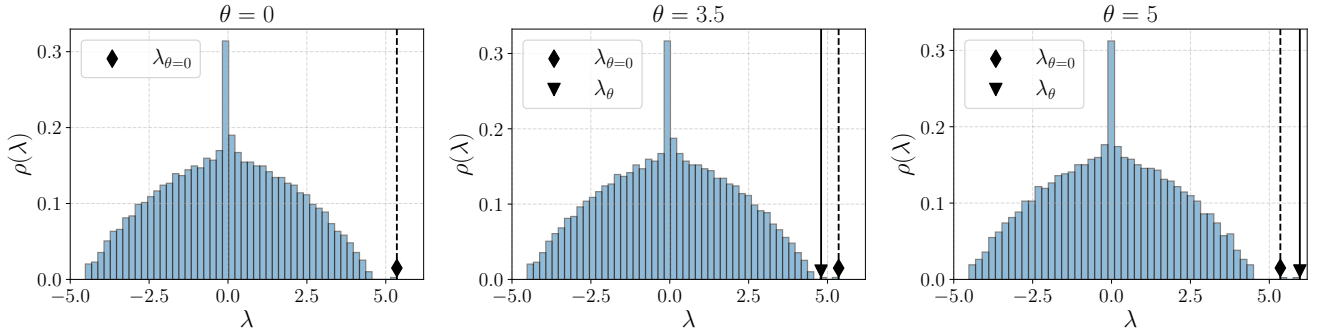


FIG. 2. Eigenvalue density of the matrix  $\mathbf{A}$  of size  $N = 2000$  as defined in Eq. (1), with  $\mathbf{J}$  a pure adjacency matrix of a Poissonian graph with average connectivity  $c = 4$  and signal  $x_i \sim \mathcal{N}(0, 1)$ . (Left) Density for  $\theta = 0$ , corresponding to  $\mathbf{A} = \mathbf{J}$ , where the structural noise eigenvalue  $\lambda_{\theta=0}$  is the sole outlier (diamond and dashed line). Matrices are generated using an unbiased configuration model algorithm that can be found in [69]. (Center) Density for  $0 < \theta < \theta_{\text{crit}}$ : the eigenvalue associated with the signal  $\lambda_\theta$  (triangle and solid line) is either an outlier such that  $\lambda_\theta < \lambda_{\theta=0}$ , or is buried in the bulk, and the top eigenvector does not correlate with the signal vector  $x$ . (Right) For  $\theta > \theta_{\text{crit}}$ , the eigenvalue associated with the signal  $\lambda_\theta$  is the top eigenvalue, and the top eigenvector correlates non-trivially with the signal vector  $x$ .

For  $\theta > \theta_{\text{crit}}$ ,  $\mathbb{E}_{\mathbf{A}}[\lambda_{\text{top}}] = \lambda_\theta$  and the average overlap  $\mathbb{E}_{\mathbf{A}}[\frac{1}{N}\langle x, v_{\text{top}} \rangle] > 0$ , indicating that signal recovery is possible via PCA. See Fig. 2 for an illustration of the mechanism. These results are proven in Appendix B.

**Result III.5** (Recovery threshold). *Under the assumption that  $\mathbb{E}_X[X] = 0$  and  $\mathbb{E}_X[X^2] = \sigma_x^2$ , the recovery threshold is given by*

$$\theta_{\text{crit}} = \frac{1}{\sigma_x^2 Q(\lambda_{\theta=0})}, \quad (25)$$

where  $\lambda_{\theta=0}$  is the structural top eigenvalue of the noise matrix  $\mathbf{J}$ , obtained by solving Eqs. (19a) and (19b) with  $\theta = 0$  [70], and the function

$$Q(\lambda_\theta) := \left\langle \int \{d\pi\}_k \{d\varrho_W\}_k \frac{1}{\lambda_\theta - \{\frac{W^2}{\omega}\}_k} \right\rangle \quad (26)$$

appears.

Consider in fact Eq. (19c), which for zero-centered spike components can be rewritten as

$$q(1 - \theta\sigma_x^2 Q(\lambda_\theta)) = 0. \quad (27)$$

Eq. (27) has two solutions:  $q = 0$ , corresponding to zero overlap between the signal and top eigenvector, and  $q \neq 0$  as long as  $\theta\sigma_x^2 Q(\lambda_\theta) = 1$ . The critical threshold  $\theta_{\text{crit}}$  has to mark the onset of a nonzero overlap, so it should be the marginal value satisfying  $\theta_{\text{crit}}\sigma_x^2 Q(\lambda_{\theta=0}) = 1$  for the top eigenvalue of  $\mathbf{J}$  in the noiseless case, leading to Eq. (25) (see Fig. 3 for a schematic illustration).

**Remark III.4** (Dense limit). In the large average connectivity limit  $c \rightarrow \infty$ , provided that  $\frac{\langle k^2 \rangle - \langle k \rangle^2}{\langle k \rangle^2} \rightarrow 0$ , the critical value  $\theta_{\text{crit}}$  in Eq. (25) converges to  $\frac{1}{\sigma_x^2}$ , the squared overlap  $\sigma_x^2 - (\theta\sigma_x^2)^{-2}$  and the top eigenvalue to  $\theta\sigma_x^2 + \frac{1}{\theta\sigma_x^2}$ , in agreement with the classical BBP result for dense real Wigner matrices [9–11]. This is shown in Appendix B 3.

#### IV. SPECIAL CASES

In this section we will specialise the results in Eq. (25) to the cases of the Poissonian setup given via Eq. (6) and to the RR setup specified by Eq. (7) for fixed noise weights. In these special cases, we are able to obtain more explicit expressions for  $\theta_{\text{crit}}$ ,  $\mathbb{E}_{\mathbf{A}}[\lambda_{\text{top}}]$  and the typical squared overlap. We will compare our prediction with the results of numerical simulations.

##### A. The Poissonian setup

Let us first specialise the relevant quantities to the Poissonian setup as corollary of our main results.

**Result IV.1** (Poissonian setup). *Assume that  $p_k$  has the form of a truncated Poisson distribution in Eq. (6). Let  $m(\lambda)$  be the solution of the self-consistency equation*

$$m(\lambda) = \left\langle \left\langle \frac{1}{\lambda - (k-1)\mathbb{E}_W[W^2]m(\lambda)} \right\rangle \right\rangle. \quad (28)$$

*Then the function  $Q$  in Eq. (26) has the explicit expression*

$$\tilde{Q}(\lambda_\theta) = \frac{c}{\bar{c}} m(\lambda_\theta) + \frac{\bar{c}^{k_{\max}}}{\Gamma k_{\max}!} \frac{1}{\lambda_\theta - k_{\max} \mathbb{E}_W[W^2]m(\lambda_\theta)}, \quad (29)$$

*and the critical value of the signal strength from Eq. (25) reads*

$$\theta_{\text{crit}} = \frac{1}{\sigma_x^2 \tilde{Q}(\lambda_{\theta=0})}. \quad (30)$$

*For  $\theta > \theta_{\text{crit}}$ , the typical value of the top eigenvalue is*

$$\mathbb{E}_{\mathbf{A}}[\lambda_{\text{top}}] = \tilde{Q}^{-1} \left( \frac{1}{\theta\sigma_x^2} \right). \quad (31)$$

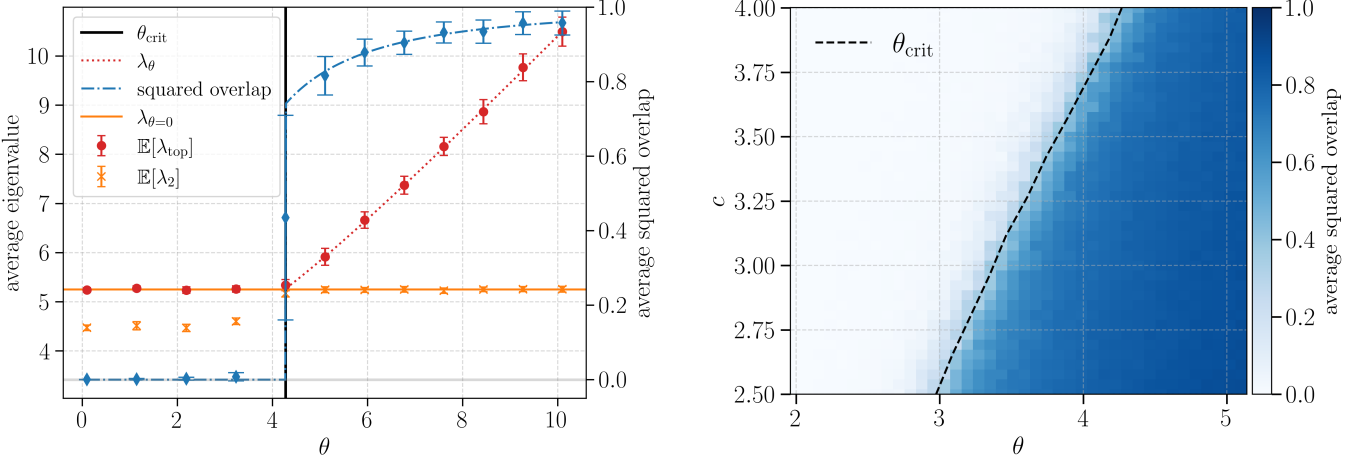


FIG. 3. Poissonian setup with  $k_{\max} = 20$ ,  $c = 4$ ,  $\varrho_W(W) = \delta(W - 1)$  and signal  $x_i \sim \mathcal{N}(0, 1)$ . All simulation results are averaged over direct diagonalisation of 25 matrices  $\mathbf{A}$  of size  $N = 10^3$  (left) and 50 matrices of size  $N = 2 \times 10^3$  (right), with standard deviation error bars. Theoretical predictions are obtained via the population dynamics algorithm described in Appendix C with population size  $N_p = 2 \times 10^5$ . (Left) Average top eigenvalue (dots) and second top eigenvalue (crosses) from direct diagonalisation for various signal strengths  $\theta$ . For  $\theta \leq \theta_{\text{crit}}$ ,  $\mathbb{E}[\lambda_{\text{top}}]$  coincides with the structural top eigenvalue  $\lambda_{\theta=0}$  of the symmetric noise matrix  $\mathbf{J}$  (orange solid line). For  $\theta > \theta_{\text{crit}}$ , the top eigenvalue correlates with the signal and its average takes the value  $\lambda_\theta$ , as predicted by Eq. (31) (red dotted line). The squared overlap in Eq. (32) (blue dashed line) also matches the simulation results (diamonds) and exhibits a discontinuity at  $\theta_{\text{crit}}$ . (Right) Heatmap of the average overlap in the  $(\theta, c)$  parameter space obtained via numerical diagonalisation. The transition value  $\theta_{\text{crit}}$  Eq. (30) (black dashed line) clearly separates the non-recovery and recovery phases.

The typical squared overlap between the signal and the top eigenvector is nonzero and equal to

$$\lim_{N \rightarrow \infty} \mathbb{E}_{\mathbf{A}} \left[ \frac{\langle x, v_{\text{top}} \rangle^2}{N^2} \right] = -\frac{1}{\sigma_x^2 \theta^2 \tilde{Q}'(\lambda_\theta)} . \quad (32)$$

For  $\theta \leq \theta_{\text{crit}}$ ,

$$\mathbb{E}_{\mathbf{A}}[\lambda_{\text{top}}] = \lambda_{\theta=0} \quad (33)$$

and the squared overlap is zero.

In Fig. 3, we present the numerical results obtained for  $c = 4$ ,  $k_{\max} = 20$ , unit bond weights  $W_{ij} = 1$  and a standard Gaussian signal  $x \sim \mathcal{N}(0, \mathbf{I}_N)$ . For  $\theta \leq \theta_{\text{crit}}$ , the average top eigenvalue, obtained by direct diagonalisation, stays constant and equal to  $\lambda_{\theta=0}$ , the structural top eigenvalue of the symmetric noise matrix  $\mathbf{J}$ . The value of  $\lambda_{\theta=0}$  is obtained via a population dynamics algorithm using a reduced  $\theta = 0$  version of the equations in Result III.1, analysed in [19]. As soon as the signal strength exceeds  $\theta_{\text{crit}}$ , the top eigenvalue becomes correlated with the signal and is well predicted by  $\lambda_\theta$  as in Eq. (31). The second largest eigenvalue, on the other hand, numerically matches the structural eigenvalue  $\lambda_{\theta=0}$  of the symmetric noise matrix  $\mathbf{J}$ . At  $\theta = \theta_{\text{crit}}$ , the squared overlap between the top eigenvector and the spike becomes nonzero, and simulation results match the prediction in Eq. (32). In the right panel, we plot the transition line associated to  $\theta_{\text{crit}}$  in Eq. (30) in the parameter space  $(\theta, c)$ : the density plot of the average overlap shows how the transition

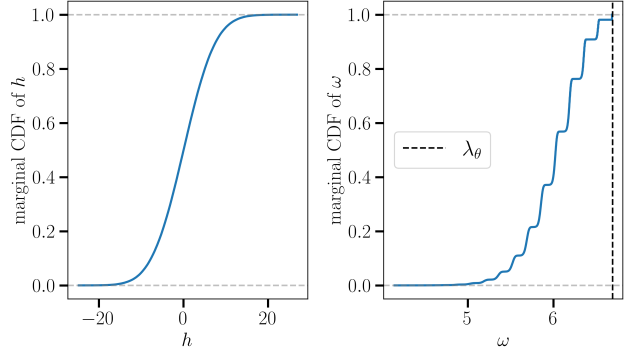


FIG. 4. Poissonian setup with  $k_{\max} = 20$ ,  $c = 4$ ,  $\varrho_W(W) = \delta(W - 1)$  and signal  $x_i \sim \mathcal{N}(0, 1)$  of strength  $\theta = 6$ . The marginal cumulative distribution functions of  $h$  and  $\omega$  are obtained via population dynamics with population size  $N_p = 2 \times 10^5$ . (Left) The marginal cumulative distribution function of the single-site bias fields  $h$ . (Right) The marginal cumulative distribution function of the single-site inverse variances  $\omega$ , where the largest value of  $\omega$  corresponds to the degree  $k = 1$  and is equal to  $\mathbb{E}_{\mathbf{A}}[\lambda_{\text{top}}] = \lambda_\theta$ .

between non-recovery (corresponding to zero overlap between the top eigenvector and signal vector) and recovery (where the overlap is of order one) takes place at  $\theta_{\text{crit}}$ .

In Fig. 4 we present the two marginals of the density  $\pi(\omega, h)$  in Eq. (19a) for  $c = 4$ ,  $k_{\max} = 20$  and  $\theta = 6$  (here in the recovery phase). Namely, we plot  $\pi(h) = \int d\omega \pi(\omega, h)$  (left) and  $\pi(\omega) = \int dh \pi(\omega, h)$  (right). Note that, in the latter, the  $k = 1$  contribution in the RHS of

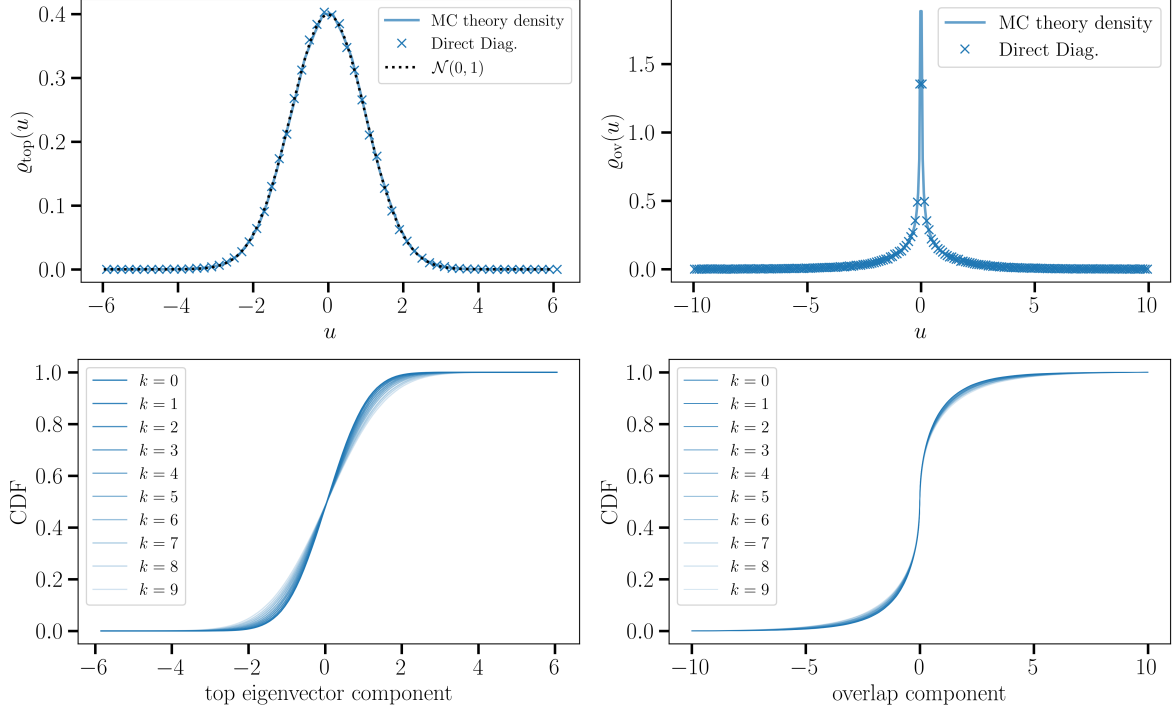


FIG. 5. Poissonian setup with  $k_{\max} = 20$ ,  $c = 4$  and  $\varrho_W(W) = \delta(W-1)$  for  $\mathbf{J}$ , and signal  $x_i \sim \mathcal{N}(0, 1)$  of strength  $\theta = 6 > \theta_{\text{crit}}$ . Plots are obtained via the population dynamics algorithm described in Appendix C with population size  $N_p = 2 \times 10^5$ . (Top left) The top eigenvector component density obtained via Eq. (21) (blue line) and direct diagonalisation (crosses). We also plot the standard Gaussian pdf (dashed line), which would be expected in case of full recovery, as a guide for the eye. (Top right) Overlap component density obtained via Eq. (22) (blue line) and direct diagonalisation (crosses). (Bottom left) Degree decomposition of the top eigenvector component cumulative distribution function (CDF) in Eq. (21). (Bottom right) Degree decomposition of the overlap component CDF in Eq. (22).

Eq. (19a) produces a  $\delta(\omega - \lambda_\theta)$ : a vertical dashed line at  $\lambda_\theta$  is added to the figure for reference.

Finally, in Fig. 5, we show the average top eigenvector component and overlap component densities (top panels), and the individual contributions to the component densities coming from nodes of degrees  $k = 0, \dots, 9$  (bottom panels). In the top panels a good agreement between the theory and direct diagonalisation results is shown.

## B. The RR setup

In the RR setup the following holds.

**Result IV.2** (Random regular setup). *Assume  $p_k$  has the form  $p_k = \delta_{k,c}$ , with  $c > 1$ , and  $\varrho_W(W) = \delta(W-1)$ . The critical value of the signal strength from Eq. (25) reads as*

$$\theta_{\text{crit}} = \frac{c(c-2)}{\sigma_x^2(c-1)}. \quad (34)$$

For  $\theta > \theta_{\text{crit}}$ , the typical value of the top eigenvalue is

$$\mathbb{E}_{\mathbf{A}}[\lambda_{\text{top}}] = \frac{c\sqrt{(\theta\sigma_x^2)^2 + 4} - (c-2)\theta\sigma_x^2}{2}. \quad (35)$$

The typical squared overlap between the signal and the top eigenvector is nonzero and equal to

$$\lim_{N \rightarrow \infty} \mathbb{E}_{\mathbf{A}} \left[ \frac{\langle x, v_{\text{top}} \rangle^2}{N^2} \right] = \frac{c\theta\sigma_x^4}{2\sqrt{(\theta\sigma_x^2)^2 + 4}} - \frac{(c-2)\sigma_x^2}{2}. \quad (36)$$

For  $\theta \leq \theta_{\text{crit}}$ , the top eigenvalue is  $\mathbb{E}_{\mathbf{A}}[\lambda_{\text{top}}] = c$  (the structural eigenvalue of a  $c$ -regular random graph) and the overlap is zero. Moreover, for  $\theta = \theta_b$  with

$$\theta_b = \frac{c-2}{\sigma_x^2\sqrt{c-1}} \leq \theta_{\text{crit}} \quad (37)$$

the eigenvalue associated with the signal detaches from the right side of the eigenvalue bulk at  $2\sqrt{c-1}$ .

We discuss Result IV.2 for a noise structure  $\mathbf{J}$  taken as a pure adjacency matrix of a  $c$ -regular random graph, i.e., by picking  $W_{ij} = 1$ . Fig. 6 shows that the predictions for the average top eigenvalue, the transition values and the typical squared overlap are in good agreement with direct diagonalisation results from large matrices for standard Gaussian-distributed spike and various values of  $\theta$  and  $c$ . In particular, the left panel of Fig. 6 shows that, for  $c = 4$ , as the signal strength  $\theta$  grows, the eigenvalue associated with the signal characterised by the formula in Eq. (35)

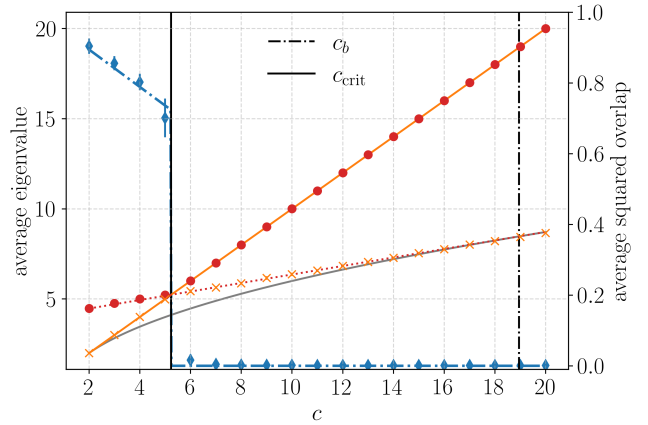
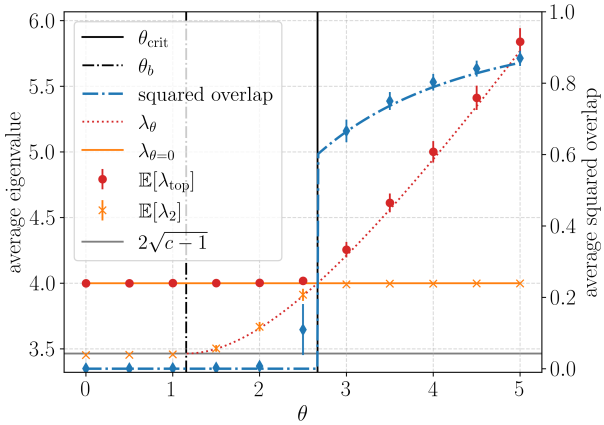


FIG. 6. Random regular setup for  $\mathbf{J}$  with  $\varrho_W(W) = \delta(W-1)$ ,  $p_k = \delta_{k,c}$  and signal  $x_i \sim \mathcal{N}(0, 1)$ . In the figures the threshold  $\theta_{\text{crit}}$  Eq. (34) (black vertical line), the average top eigenvalue (dots) and second top eigenvalue (crosses) from direct diagonalisation for various signal strengths  $\theta$  are given. For  $\theta \leq \theta_{\text{crit}}$ , the structural outlier eigenvalue  $\lambda_{\theta=0} = c$  of the symmetric noise matrix  $\mathbf{J}$  (orange solid line) is the top eigenvalue of  $\mathbf{A}$ . For  $\theta > \theta_{\text{crit}}$ , the eigenvalue associated with the signal  $\lambda_\theta$  dominates, as predicted by Eq. (35) (red dotted line). The squared overlap in Eq. (36) (blue dashed line) matches the simulation results (diamonds) and jumps from zero to a nonzero value at  $\theta_{\text{crit}}$ . At  $\theta_b$  Eq. (37), the eigenvalue associated with the signal  $\lambda_\theta$  detaches from the bulk and is the second top eigenvalue for  $\theta_b < \theta < \theta_{\text{crit}}$ . The average overlap values from those experiments are reported on the left axis (blue diamonds). (Left) Results varying  $\theta$  at fixed  $c = 4$ . (Right) Results varying  $c$  at fixed  $\theta = 4$ . All simulation results are averaged over direct diagonalisation of 10 matrices  $\mathbf{A}$  of size  $N = 2 \times 10^3$ , with standard deviation error bars.

detaches from the bulk at  $\theta_b$  in Eq. (37) and overtakes the structural eigenvalue  $\lambda_{\theta=0} = c$  at  $\theta_{\text{crit}}$  in Eq. (34), where for  $\theta > \theta_{\text{crit}}$  the squared overlap between the top eigenvector and signal becomes nonzero and is predicted by Eq. (36).

On the right side of Fig. 6 we fix  $\theta$  and observe that for small noise density  $c$  the signal eigenvalue  $\lambda_\theta$  dominates. As  $c$  grows, it is overtaken by  $\lambda_{\theta=0} = c$  with the squared overlap between the top eigenvector and signal in Eq. (36) becomes zero at

$$\theta_{\text{crit}} = \frac{2 + \theta \sigma_x^2 + \sqrt{4 + \theta^2 \sigma_x^4}}{2},$$

and  $\lambda_\theta$  is absorbed by the bulk at

$$c_b = \frac{1}{4} \left( \theta \sigma_x^2 + \sqrt{\theta^2 \sigma_x^4 + 4} \right)^2 + 1.$$

The numerical results are given for  $\theta = 4$ .

Finally, Fig. 7 shows a phase diagram in the  $(\theta, c)$  parameter space with signal  $x \sim \mathcal{N}(\mathbf{0}, \mathbf{I}_N)$ . We show the squared overlap computed using direct diagonalisation of large matrices. In phase A, the top eigenvalue associated with the signal is buried in the bulk, whereas in phase B it has detached from the bulk but remains smaller than the structural eigenvalue at  $\mathbb{E}_{\mathbf{A}}[\lambda_{\text{top}}] = c$ . Finally, in phase C the eigenvalue associated with the signal is the top eigenvalue predicted by Eq. (35) and the squared overlap of the top eigenvector with the signal is of order one.

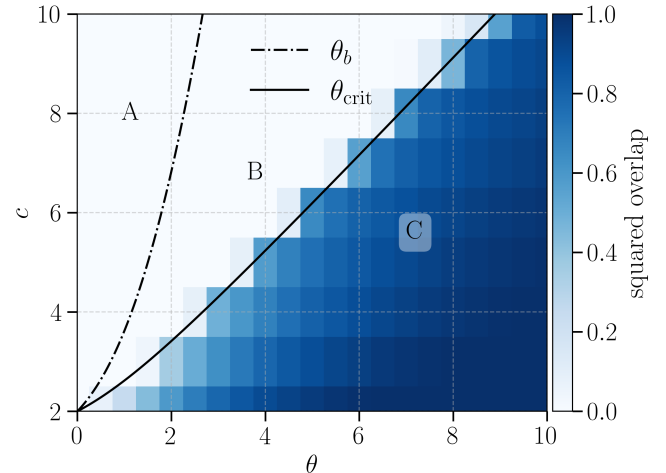


FIG. 7. Random regular setup with  $\varrho_W(W) = \delta(W-1)$  and signal  $x_i \sim \mathcal{N}(0, 1)$ . The average squared overlap is given in the  $(\theta, c)$  parameter space as obtained via numerical diagonalisation of five instances of size  $N = 10^3$ . The dashed line corresponds to  $\theta_b$  in Eq. (37), where the signal eigenvalue detaches from the bulk. The solid line shows  $\theta_{\text{crit}}$  in Eq. (34), where the signal eigenvalue becomes the top eigenvalue.

## V. CONCLUSIONS AND OUTLOOK

We have studied the problem of recovering a rank-one signal  $\frac{\theta}{N} \mathbf{x} \mathbf{x}^\top \in \mathbb{R}^{N \times N}$  from the off-diagonal elements of the noisy observation  $\mathbf{J} + \frac{\theta}{N} \mathbf{x} \mathbf{x}^\top$ , where the noise matrix  $\mathbf{J} \in \mathbb{R}^{N \times N}$  is sparse. The noise is modeled as a sparse symmetric weighted adjacency matrix of a graph constructed from the configuration model with *any* degree

distribution  $p_k$  with bounded maximum degree. From a technical standpoint, our main contribution is the extension of the replica formalism used to calculate spectral properties of large matrices with sparse structure in [15, 17, 18, 20, 21, 71] to the class of spiked matrix models. The non-trivial extension, i.e., the addition of the perturbation  $\frac{\theta}{N}xx^\top$  in the model, required the introduction of an auxiliary parameter  $q$ , identified as the overlap between the signal and top eigenvector, and modifications to recursive distributional equations to account for a spike-induced shift in the recursions that depends on the signal strength  $\theta$  and the distribution of the spike components. We also derived the density of the top eigenvector components as in previous work along with a novel observable: the overlap component density; its average also quantifies the average overlap between the top eigenvector and signal vector.

From a practical standpoint, the main contribution is the identification of an the analogue of the BBP transition for rank-one signal recovery with a sparse noise matrix, constructed from the configuration model with *any* degree distribution  $p_k$  with finite mean and bounded maximal degree. This transition, that occurs in terms of the signal-to-noise ratio parameter  $\theta$  at a given value  $\theta_{\text{crit}}$ , is such that for  $\theta > \theta_{\text{crit}}$  the rank-one signal correlates non-trivially with the top eigenvector. We provide results for two noise models and show excellent agreement with direct diagonalisation. For noise modelled as an adjacency matrix of a configuration model with Poissonian connectivity, we determine explicitly the critical transition value, typical top eigenvalue, typical squared overlap and the top eigenvector component density in the recovery phase. If  $\mathbf{J}$  is the pure adjacency matrix of a  $c$ -random regular graph, we obtain analytic formulae for the typical top eigenvalue associated with the signal, the typical squared overlap along with two thresholds: the BBP analogue transition value, at which the eigenvalue associated with the signal overtakes the structural outlier eigenvalue and the top eigenvector correlates non-trivially with the signal, and a second threshold where the eigenvalue associated with the signal detaches from the right bulk edge and becomes an outlier.

As expected, in the large connectivity limit our results converge to the known BBP-like transition, the top eigenvalue and squared overlap for dense real Wigner matrices [9–11].

A natural extension would be to consider sparse signal models that would contribute to the growing literature of recovery thresholds for Sparse PCA. Extensions to a configuration model for the noise matrix with correlated degrees, higher-rank signals, structured priors on the signal components or heavy-tailed assumptions on either are also interesting avenues for future work. A localisation phenomenon is observed for zero-centered Gaussian bond weights, where the top eigenvector correlates with the high-degree nodes rather than aligning with the signal: a more thorough analysis of the nature of the localisation is left for future work. Finally, in the current setting,

there is a phase where the eigenvalue associated with the signal is an outlier but smaller than the structural top eigenvalue associated with the noise, which motivates an analysis of the second top eigenpair statistics as in [20] in the context of signal recovery via top principal components of the observed matrix.

## ACKNOWLEDGMENTS

The authors thank Preben Forer, Sebastian Goldt, Barak Budnick and Giovanni Piccioli for helpful discussions. P.V. acknowledges support from UKRI FLF Scheme (No. MR/X023028/1).

## Appendix A: Replica derivation

In this Appendix, we outline the derivations in the replica calculation. The object of main interest is the replicated partition function  $\mathbb{E}_{\mathbf{A}}[(Z_{\beta}[\mathbf{A}; tF])^n]$ , with  $Z_{\beta}[\mathbf{A}; tF]$  given by Eq. (13), namely

$$Z_{\beta}[\mathbf{A}; tF] := \int d\mathbf{v} \exp \left[ \frac{\beta}{2} \langle \mathbf{v}, \mathbf{A}\mathbf{v} \rangle + \beta tN F(u, \mathbf{v}, \mathbf{x}) \right] \delta(\|\mathbf{v}\|^2 - N) , \quad (\text{A1})$$

and  $\mathbf{A} = \mathbf{C} \odot \mathbf{W} + \frac{\theta}{N} \mathbf{x}\mathbf{x}^{\top}$ . We will specifically focus on the cases in which  $F$  can be written as

$$F(u, \mathbf{v}, \mathbf{x}) = \frac{1}{N} \sum_i f(u, v_i, x_i) . \quad (\text{A2})$$

Recall the noise model construction in Eq. (3) and Eq. (4). For the purpose of the calculation, we follow a shortcut procedure whose validity has been proved in Appendix B of [19]. It consists of the following steps:

1. Replace the true connectivity distribution in Eq. (4) with

$$P_c(\mathbf{C}|k) \propto \prod_{i=1}^N \mathbb{I} \left( \sum_j c_{ij} = k_i \right) \delta_{c_{ii}, 0} \prod_{j>i} \left[ \frac{c}{N} \delta_{c_{ij}, 1} + \left(1 - \frac{c}{N}\right) \delta_{c_{ij}, 0} \right] , \quad (\text{A3})$$

where  $\mathbf{k} = (k_i)_{i=1}^N$  is a vector of integers  $k_i$  i.i.d. sampled with distribution  $p_k$ , and  $c := \langle k \rangle = \sum_k k p_k$ . This replacement has not changed the probability of sampling a matrix  $\mathbf{C}$  in the ensemble, as the extra factor is constant for the matrices in the ensemble.

2. Drop the degree constraint term  $\prod_i \mathbb{I} \left( \sum_j c_{ij} = k_i \right)$  altogether. The resulting distribution

$$P_{ER}(\mathbf{C}) = \prod_{i=1}^N \delta_{c_{ii}, 0} \prod_{j>i} \left[ \frac{c}{N} \delta_{c_{ij}, 1} + \left(1 - \frac{c}{N}\right) \delta_{c_{ij}, 0} \right] , \quad (\text{A4})$$

now corresponds to a sparse Erdős-Rényi (ER) graph with average connectivity  $c$ . While the distribution (A4) on adjacency matrices  $\mathbf{C}$  is no longer equivalent to either (A3) or (4), it will produce a final result for the average replicated partition function  $\mathbb{E}_{\mathbf{A}}[(Z_{\beta}[\mathbf{A}; tF])^n]$  (see Eq. (A35) below) involving the Poissonian degree distribution  $p_k^{(c)}$  characteristic of ER graphs.

3. The final result for *generic* degree distributions  $p_k$  cited in the main text (19a) follows by simply replacing  $p_k^{(c)}$  with  $p_k$  in the final formulas. The validity of this shortcut was demonstrated in Appendix B of [19].

By keeping the previous observation in mind, let us start by replicating  $Z_{\beta}[\mathbf{A}; tF]$  and averaging over  $\mathbf{A}$ . We get

$$\begin{aligned} \mathbb{E}_{\mathbf{A}}[(Z_{\beta}[\mathbf{A}; tF])^n] &\propto \left( \prod_{a=1}^n \int \delta(\|\mathbf{v}_a\|^2 - N) d\mathbf{v}_a \right) \mathbb{E}_{\mathbf{A}} \left[ \exp \left( \frac{\beta}{2} \sum_{a=1}^n \langle \mathbf{v}_a, \mathbf{A}\mathbf{v}_a \rangle + \beta tN \sum_a F(u, \mathbf{v}_a, \mathbf{x}) \right) \right] \\ &= \left( \prod_{a=1}^n \int d\mathbf{v}_a \int d\lambda_a \right) \mathbb{E}_{\mathbf{A}} \left[ \exp \left( i \frac{N\beta}{2} \sum_a \lambda_a - i\beta \sum_{ai} v_{ai}^2 \lambda_a + \frac{\beta}{2} \sum_{a=1}^n \langle \mathbf{v}_a, \mathbf{A}\mathbf{v}_a \rangle + \beta tN \sum_a F(u, \mathbf{v}_a, \mathbf{x}) \right) \right] . \end{aligned} \quad (\text{A5})$$

We can perform immediately the expectation over  $\mathbf{J} = \mathbf{C} \odot \mathbf{W}$  [15] by invoking the law of total expectation  $\mathbb{E}_{\mathbf{A}}[\bullet] = \mathbb{E}_{\mathbf{x}}[\mathbb{E}_{\mathbf{J}|\mathbf{x}}[\bullet]]$ , with  $\mathbf{C}$  sampled from the ER distribution in Eq. (A4). By using Appendix D of [72]

$$\mathbb{E}_{\mathbf{J}|\mathbf{x}} \left[ \exp \left( \frac{\beta}{2} \sum_{a=1}^n \langle \mathbf{v}_a, \mathbf{J}\mathbf{v}_a \rangle \right) \right] = \left( \frac{c}{2N} \sum_{ij} \left( \mathbb{E}_{\mathbf{W}}[e^{\beta W \langle \mathbf{v}_i, \mathbf{v}_j \rangle}] - 1 \right) \right) \quad (\text{A6})$$

we obtain

$$\mathbb{E}_{\mathbf{x}} \left[ \mathbb{E}_{\mathbf{J}|\mathbf{x}} \left[ \exp \left( \frac{\beta}{2} \sum_{a=1}^n \langle \mathbf{v}_a, \mathbf{A}\mathbf{v}_a \rangle + \beta tN \sum_a F(u, \mathbf{v}_a, \mathbf{x}) \right) \right] \right]$$

$$\begin{aligned}
&= \mathbb{E}_x \left[ \exp \left( \frac{c}{2N} \sum_{ij} \left( \mathbb{E}_W[e^{\beta W \langle \mathbf{v}_i, \mathbf{v}_j \rangle}] - 1 \right) + \frac{\theta\beta}{2N} \sum_a \langle \mathbf{v}_a, \mathbf{x} \rangle^2 + \beta t N \sum_a F(u, \mathbf{v}_a, \mathbf{x}) \right) \right] \\
&= \exp \left( \frac{c}{2N} \sum_{ij} \left( \mathbb{E}_W[e^{\beta W \langle \mathbf{v}_i, \mathbf{v}_j \rangle}] - 1 \right) \right) \mathbb{E}_x \left[ \exp \left( \frac{\theta\beta}{2N} \sum_a \langle \mathbf{v}_a, \mathbf{x} \rangle^2 + \beta t N \sum_a F(u, \mathbf{v}_a, \mathbf{x}) \right) \right], \quad (\text{A7})
\end{aligned}$$

where  $\mathbf{v}_i := (v_{ia})_{a \in [n]}$  is the  $n$ -replicated  $i$ th-component of  $\mathbf{v}$  [72] and we have denoted by  $W$  a random variable with distribution  $\varrho_W$ . Let us now introduce the following (normalized) functional order parameters

$$\varphi(\mathbf{v}) := \frac{1}{N} \sum_i \delta^{(n)}(\mathbf{v} - \mathbf{v}_i), \quad \psi(\mathbf{v}) := \frac{1}{N} \sum_{i=1}^N \delta^{(n)}(\mathbf{v} - x_i \mathbf{v}_i), \quad (\text{A8})$$

where  $\delta^{(n)}$  is the  $n$ -dimensional Dirac delta function  $\delta^{(n)}(\mathbf{v} - \mathbf{v}_i) = \prod_{a=1}^n \delta(v_a - v_{ia})$ , by means of a suitable Fourier representation

$$\begin{aligned}
1 &= \iint \mathcal{D}\psi \mathcal{D}\hat{\psi} \exp \left( -i \int \hat{\psi}(\mathbf{v}) \left( N\psi(\mathbf{v}) - \sum_i \delta^{(n)}(\mathbf{v} - x_i \mathbf{v}_i) \right) d\mathbf{v} \right) \iint \mathcal{D}\varphi \mathcal{D}\hat{\varphi} \exp \left( -i \int \hat{\varphi}(\mathbf{v}) \left( N\varphi(\mathbf{v}) - \sum_i \delta^{(n)}(\mathbf{v} - \mathbf{v}_i) \right) d\mathbf{v} \right) \\
&= \iint \mathcal{D}\psi \mathcal{D}\hat{\psi} \iint \mathcal{D}\varphi \mathcal{D}\hat{\varphi} \exp \left( i \sum_i \hat{\psi}(x_i \mathbf{v}_i) + i \sum_i \hat{\varphi}(\mathbf{v}_i) - iN \int (\hat{\psi}(\mathbf{v})\psi(\mathbf{v}) + \hat{\varphi}(\mathbf{v})\varphi(\mathbf{v})) d\mathbf{v} \right), \quad (\text{A9})
\end{aligned}$$

where  $d\mathbf{v} = \prod_{a=1}^n dv_a$ . Inserting this representation of the unity within the argument of  $\mathbb{E}_x[\bullet]$  in Eq. (A7):

$$\begin{aligned}
&\exp \left( \frac{c}{2N} \sum_{ij} \left( \mathbb{E}_W[e^{\beta W \langle \mathbf{v}_i, \mathbf{v}_j \rangle}] - 1 \right) \right) \mathbb{E}_x \left[ \exp \left( \frac{\theta\beta}{2N} \sum_a \langle \mathbf{v}_a, \mathbf{x} \rangle^2 + \beta t \sum_a \sum_i f(u, v_{ia}, x_i) \right) \right] \\
&= \exp \left( \frac{c}{2N} \sum_{ij} \left( \mathbb{E}_W[e^{\beta W \langle \mathbf{v}_i, \mathbf{v}_j \rangle}] - 1 \right) \right) \mathbb{E}_x \left[ \iint \mathcal{D}\psi \mathcal{D}\hat{\psi} \iint \mathcal{D}\varphi \mathcal{D}\hat{\varphi} \exp \left( i \sum_i (\hat{\psi}(x_i \mathbf{v}_i) + \hat{\varphi}(\mathbf{v}_i)) \right. \right. \\
&\quad \left. \left. - iN \int (\hat{\psi}(\mathbf{v})\psi(\mathbf{v}) + \hat{\varphi}(\mathbf{v})\varphi(\mathbf{v})) d\mathbf{v} + \frac{\theta\beta}{2N} \sum_a \langle \mathbf{v}_a, \mathbf{x} \rangle^2 + \beta t \sum_a \sum_i f(u, v_{ia}, x_i) \right) \right] \\
&= \iint \mathcal{D}\varphi \mathcal{D}\hat{\varphi} \iint \mathcal{D}\psi \mathcal{D}\hat{\psi} \exp \left( \frac{\theta\beta N}{2} \iint \langle \mathbf{v}, \mathbf{v}' \rangle \psi(\mathbf{v})\psi(\mathbf{v}') d\mathbf{v} d\mathbf{v}' \right) \\
&\quad \times \exp \left( \frac{cN}{2} \iint d\mathbf{v} d\mathbf{v}' \varphi(\mathbf{v})\varphi(\mathbf{v}') (\mathbb{E}_W[e^{\beta W \langle \mathbf{v}, \mathbf{v}' \rangle}] - 1) - iN \int (\hat{\psi}(\mathbf{v})\psi(\mathbf{v}) + \hat{\varphi}(\mathbf{v})\varphi(\mathbf{v})) d\mathbf{v} \right) \\
&\quad \times \mathbb{E}_x \left[ \exp \left( \sum_i \left( i\hat{\psi}(x_i \mathbf{v}_i) + i\hat{\varphi}(\mathbf{v}_i) + \beta t \sum_a f(u, v_{ia}, x_i) \right) \right) \right]. \quad (\text{A10})
\end{aligned}$$

The replicated partition function now reads as

$$\begin{aligned}
\mathbb{E}_{\mathbf{A}} [(Z_{\beta}[\mathbf{A}; tF])^n] &= \int d\lambda \iint \mathcal{D}\psi \mathcal{D}\hat{\psi} \iint \mathcal{D}\varphi \mathcal{D}\hat{\varphi} \\
&\quad \times \exp \left( -iN \int \varphi(\mathbf{v})\hat{\varphi}(\mathbf{v}) d\mathbf{v} + \frac{cN}{2} \iint \varphi(\mathbf{v})\varphi(\mathbf{v}') (\mathbb{E}_W[e^{\beta W \langle \mathbf{v}, \mathbf{v}' \rangle}] - 1) d\mathbf{v} d\mathbf{v}' + i\frac{N\beta}{2} \sum_a \lambda_a \right) \\
&\quad \times \exp \left( -iN \int \psi(\mathbf{v})\hat{\psi}(\mathbf{v}) d\mathbf{v} + \frac{\theta\beta N}{2} \iint \langle \mathbf{v}, \mathbf{v}' \rangle \psi(\mathbf{v})\psi(\mathbf{v}') d\mathbf{v}' d\mathbf{v} \right) \\
&\quad \times \left[ \mathbb{E}_X \int d\mathbf{v} \exp \left( -\frac{i\beta}{2} \sum_a \lambda_a v_a^2 + i\hat{\varphi}(\mathbf{v}) + i\hat{\psi}(X\mathbf{v}) + \beta t \sum_a f(u, v_a, X) \right) \right]^N, \quad (\text{A11})
\end{aligned}$$

where  $\lambda := (\lambda_a)_{a \in [n]}$  and  $X \sim \varrho_x$  has the same distribution as each i.i.d. entry of  $x$ . Let us now introduce

$$I_f[\hat{\varphi}, \hat{\psi}, \lambda; t] := \frac{1}{\beta n} \ln \mathbb{E}_X \left[ \int d\mathbf{v} \exp \left( -\frac{i\beta}{2} \sum_a \lambda_a v_a^2 + i\hat{\varphi}(\mathbf{v}) + i\hat{\psi}(X\mathbf{v}) + \beta t \sum_a f(u, v_a, X) \right) \right]. \quad (\text{A12})$$

The functional integral (A11) can now be evaluated for large  $N$  by means of a saddle-point approximation

$$\mathbb{E}_{\mathbf{A}}[(Z_{\beta}[\mathbf{A}; tF])^n] \propto \int d\lambda \iint \mathcal{D}\psi \mathcal{D}\hat{\psi} \iint \mathcal{D}\varphi \mathcal{D}\hat{\varphi} e^{N\mathcal{S}_{\beta}[\varphi, \hat{\varphi}, \psi, \hat{\psi}; \lambda; t, f]} \approx e^{N\mathcal{S}_{\beta}[\varphi^*, \hat{\varphi}^*, \psi^*, \hat{\psi}^*, \lambda^*(t); t, f]}, \quad (\text{A13})$$

where the action reads as

$$\begin{aligned} \mathcal{S}_{\beta}[\varphi, \hat{\varphi}, \psi, \hat{\psi}; \lambda; t, f] &:= -i \int (\varphi(\mathbf{v})\hat{\varphi}(\mathbf{v}) + \psi(\mathbf{v})\hat{\psi}(\mathbf{v})) d\mathbf{v} + \frac{c}{2} \iint \varphi(\mathbf{v})\varphi(\mathbf{v}') (\mathbb{E}_W[e^{\beta W\langle \mathbf{v}, \mathbf{v}' \rangle}] - 1) d\mathbf{v} d\mathbf{v}' \\ &\quad + i\frac{\beta}{2} \sum_a \lambda_a + \frac{\theta\beta}{2} \iint \langle \mathbf{v}, \mathbf{v}' \rangle \psi(\mathbf{v})\psi(\mathbf{v}') d\mathbf{v}' d\mathbf{v} + \beta n I_f[\hat{\varphi}, \hat{\psi}, \lambda; t]. \end{aligned} \quad (\text{A14})$$

The saddle-point values of the fields and the multipliers are determined from the following saddle-point equations, obtained differentiating the action w.r.t.  $\varphi, \hat{\varphi}, \psi, \hat{\psi}$  and  $\lambda_a$  and setting the derivatives equal to zero:

$$1 = \frac{\mathbb{E}_X \int d\mathbf{v} v_a^2 \exp\left(-\frac{\beta}{2} \sum_a \lambda_a^*(t) v_a^2 + i\hat{\varphi}^*(\mathbf{v}) + i\hat{\psi}^*(X\mathbf{v}) + \beta t \sum_a f(u, v_a, X)\right)}{\mathbb{E}_X \int d\mathbf{v}' \exp\left(-\frac{\beta}{2} \sum_a \lambda_a^*(t) v_a'^2 + i\hat{\varphi}^*(\mathbf{v}') + i\hat{\psi}^*(X\mathbf{v}') + \beta t \sum_a f(u, v_a', X)\right)}, \quad (\text{A15})$$

$$i\hat{\varphi}^*(\mathbf{v}) = c \int \varphi^*(\mathbf{v}') (\mathbb{E}_W[e^{\beta W\langle \mathbf{v}, \mathbf{v}' \rangle}] - 1) d\mathbf{v}', \quad (\text{A16})$$

$$\varphi^*(\mathbf{v}) = \frac{\mathbb{E}_X \left[ \exp\left(-\frac{\beta}{2} \sum_a \lambda_a^*(t) v_a^2 + i\hat{\varphi}^*(\mathbf{v}) + i\hat{\psi}^*(X\mathbf{v}) + \beta t \sum_a f(u, v_a, X)\right) \right]}{\mathbb{E}_X \left[ \int d\mathbf{v}' \exp\left(-\frac{\beta}{2} \sum_a \lambda_a^*(t) v_a'^2 + i\hat{\varphi}^*(\mathbf{v}') + i\hat{\psi}^*(X\mathbf{v}') + \beta t \sum_a f(u, v_a', X)\right) \right]}, \quad (\text{A17})$$

$$i\hat{\psi}^*(\mathbf{v}) = \theta\beta \int \langle \mathbf{v}, \mathbf{v}' \rangle \psi^*(\mathbf{v}') d\mathbf{v}', \quad (\text{A18})$$

$$\psi^*(\mathbf{v}) = \frac{\mathbb{E}_X \left[ |X|^{-n} \exp\left(-\frac{\beta}{2X^2} \sum_a \lambda_a^*(t) v_a^2 + i\hat{\varphi}^*(X^{-1}\mathbf{v}) + i\hat{\psi}^*(\mathbf{v}) + \beta t \sum_a f(u, X^{-1}v_a, X)\right) \right]}{\mathbb{E}_X \left[ \int d\mathbf{v}' \exp\left(-\frac{\beta}{2} \sum_a \lambda_a^*(t) v_a'^2 + i\hat{\varphi}^*(\mathbf{v}') + i\hat{\psi}^*(X\mathbf{v}') + \beta t \sum_a f(u, v_a', X)\right) \right]}, \quad (\text{A19})$$

the first one to be intended for all  $a = 1, \dots, n$ . We have redefined  $i\lambda_a \rightarrow \lambda_a$  and explicitly highlighted the  $t$ -dependence of the multipliers  $\lambda_a^*$  at the saddle-point, which follows from the constraint (A15) and will be important in the following. It follows from (A18) that  $i\hat{\psi}^*(\mathbf{v})$  must be a linear function of its arguments

$$i\hat{\psi}^*(\mathbf{v}) = \theta\beta \langle \mathbf{q}(t), \mathbf{v} \rangle, \quad \mathbf{q}(t) := \int \mathbf{v} \psi^*(\mathbf{v}) d\mathbf{v} \quad (\text{A20})$$

in terms of a  $t$ -dependent  $n$ -dimensional vector  $\mathbf{q}(t) = (q_a(t))$  for  $a = 1, \dots, n$ . Multiplying Eq. (A19) by  $v_a$  and integrating, we find that  $\mathbf{q}(t)$  must satisfy component-wise the self-consistency equation

$$\mathbf{q}(t) = \frac{\mathbb{E}_X \left[ \text{sign}(X^n) X \int d\mathbf{v} \mathbf{v} \exp\left(-\frac{\beta}{2} \sum_a \lambda_a^*(t) v_a^2 + i\hat{\varphi}^*(\mathbf{v}) + \theta\beta X \langle \mathbf{q}(t), \mathbf{v} \rangle + \beta t \sum_a f(u, v_a, X)\right) \right]}{\mathbb{E}_X \left[ \int d\mathbf{v}' \exp\left(-\frac{\beta}{2} \sum_a \lambda_a^*(t) v_a'^2 + i\hat{\varphi}^*(\mathbf{v}') + \theta\beta X \langle \mathbf{q}(t), \mathbf{v}' \rangle + \beta t \sum_a f(u, v_a', X)\right) \right]}, \quad (\text{A21})$$

while the saddle-point equations above can be reduced to

$$1 = \frac{\mathbb{E}_X \int d\mathbf{v} v_a^2 \exp\left(-\frac{\beta}{2} \sum_a \lambda_a^*(t) v_a^2 + i\hat{\varphi}^*(\mathbf{v}) + X\theta\beta \langle \mathbf{q}(t), \mathbf{v} \rangle + \beta t \sum_a f(u, v_a, X)\right)}{\mathbb{E}_X \int d\mathbf{v}' \exp\left(-\frac{\beta}{2} \sum_a \lambda_a^*(t) v_a'^2 + i\hat{\varphi}^*(\mathbf{v}') + \theta\beta X \langle \mathbf{q}(t), \mathbf{v}' \rangle + \beta t \sum_a f(u, v_a', X)\right)}, \quad (\text{A22})$$

$$i\hat{\varphi}^*(\mathbf{v}) = c \int \varphi^*(\mathbf{v}') (\mathbb{E}_W[e^{\beta W\langle \mathbf{v}, \mathbf{v}' \rangle}] - 1) d\mathbf{v}', \quad (\text{A23})$$

$$\varphi^*(\mathbf{v}) = \frac{\mathbb{E}_X \left[ \exp\left(-\frac{\beta}{2} \sum_a \lambda_a^*(t) v_a^2 + i\hat{\varphi}^*(\mathbf{v}) + \theta\beta X \langle \mathbf{q}(t), \mathbf{v} \rangle + \beta t \sum_a f(u, v_a, X)\right) \right]}{\mathbb{E}_X \left[ \int d\mathbf{v}' \exp\left(-\frac{\beta}{2} \sum_a \lambda_a^*(t) v_a'^2 + i\hat{\varphi}^*(\mathbf{v}') + \theta\beta X \langle \mathbf{q}(t), \mathbf{v}' \rangle + \beta t \sum_a f(u, v_a', X)\right) \right]}. \quad (\text{A24})$$

Now, recall from Eq. (14) that we will be interested in extracting the limit  $n \rightarrow 0$  followed by the limit  $\beta \rightarrow \infty$  of the action (A14) evaluated at the saddle-point values of the fields and multipliers. To extract these limits, it is necessary

to postulate what kind of invariance the action and the saddle-point fields will enjoy with respect to permutation of replica indices. In the random matrix literature, it has been established [15, 19–21, 72, 73] that a solution that preserves the symmetry among replicas is exact for extreme value problems on sparse random matrices [74]. In this paper, we indeed follow the strategy introduced in [15, 75] and represent the fields at the saddle-point as superposition of Gaussians with fluctuating mean and variance, i.e.

$$\lambda_a^*(t) \equiv \lambda_\theta(t) \quad \forall a, \quad (A25a)$$

$$\mathbf{q}(t) = q(t)\mathbf{1}_n, \quad (A25b)$$

$$\varphi^*(\mathbf{v}) = \int \frac{e^{-\frac{\beta\omega}{2}\|\mathbf{v}\|^2 + \beta h\langle \mathbf{1}_n, \mathbf{v} \rangle}}{\mathcal{Z}_\beta^n(\omega, h)} \pi(\omega, h) d\omega d h, \quad (A25c)$$

$$i\hat{\varphi}^*(\mathbf{v}) = \hat{\phi} \int e^{\frac{\beta\hat{\omega}}{2}\|\mathbf{v}\|^2 + \beta\hat{h}\langle \mathbf{1}_n, \mathbf{v} \rangle} \hat{\pi}(\hat{\omega}, \hat{h}) d\hat{\omega} d\hat{h}, \quad (A25d)$$

for some joint probability densities  $\pi$  and  $\hat{\pi}$  defined and normalized for  $\omega, \hat{\omega} > 0$  and  $h, \hat{h} \in \mathbb{R}$ , and for  $\mathcal{Z}_\beta(a, b) := \sqrt{\frac{2\pi}{a\beta}} \exp\left(\frac{\beta b^2}{2a}\right)$ . The constant  $\hat{\phi}$  is introduced as the conjugate field  $i\hat{\varphi}^*(\mathbf{v})$  does not have the interpretation of a density (as opposed to  $\varphi^*$  from (A8)) and thus needs not be normalised.

We now insert the ansatz above into the action (A14) evaluated at the saddle-point and compute the corresponding  $\mathbf{v}$  and  $\mathbf{v}'$  Gaussian integrals as required. For instance

$$\begin{aligned} -i \int d\mathbf{v} \varphi^*(\mathbf{v}) \hat{\varphi}^*(\mathbf{v}) &\mapsto -\hat{\phi} \int d\pi d\hat{\pi} \int d\mathbf{v} \prod_a \frac{e^{-\frac{\beta}{2}(\omega-\hat{\omega})v_a^2 + \beta(h+\hat{h})v_a}}{\mathcal{Z}_\beta(\omega, h)} \\ &= -\hat{\phi} \int d\pi d\hat{\pi} \left[ \frac{\mathcal{Z}_\beta(\omega - \hat{\omega}, h + \hat{h})}{\mathcal{Z}_\beta(\omega, h)} \right]^n = -\hat{\phi} - \hat{\phi} n \int d\pi d\hat{\pi} \ln \left[ \frac{\mathcal{Z}_\beta(\omega - \hat{\omega}, h + \hat{h})}{\mathcal{Z}_\beta(\omega, h)} \right] + o(n), \end{aligned}$$

where in the last step we have extracted the  $n \rightarrow 0$  asymptotic behaviour using  $A^n \sim 1 + n \ln A$  and the fact that both  $\pi$  and  $\hat{\pi}$  are normalised to one. Similarly from (A12) and with some notation redundancy,

$$\begin{aligned} \beta I_f[\hat{\pi}, q(t), \lambda_\theta(t); t] &:= \lim_{n \rightarrow 0} \frac{\beta n I_f[\hat{\varphi}^*, \hat{\psi}^*, \lambda^*(t); t] - \hat{\phi}}{n} \\ &= \lim_{n \rightarrow 0} \frac{1}{n} \ln \mathbb{E}_X \left[ \int d\mathbf{v} e^{-\frac{\beta}{2}\lambda_\theta(t) \sum_a v_a^2 + i\hat{\psi}^*(X\mathbf{v}) + \beta t \sum_a f(u, v_a, X) + i\hat{\varphi}^*(\mathbf{v}) - \hat{\phi}} \right] \\ &= \lim_{n \rightarrow 0} \frac{1}{n} \ln \mathbb{E}_X \sum_{s=0}^{\infty} \frac{\hat{\phi}^s e^{-\hat{\phi}}}{s!} \int \{d\hat{\pi}\}_s \int d\mathbf{v} \prod_{a=1}^s \left( e^{\frac{\beta}{2}\hat{\omega}v_a^2 + \beta\hat{h}v_a} \right) e^{-\frac{\beta}{2}\lambda_\theta(t) \sum_a v_a^2 + \beta t \sum_a f(u, v_a, X) + \beta\theta X \langle \mathbf{q}(t), \mathbf{v} \rangle} \\ &= \lim_{n \rightarrow 0} \frac{1}{n} \ln \mathbb{E}_X \sum_{s=0}^{\infty} \frac{\hat{\phi}^s e^{-\hat{\phi}}}{s!} \int \{d\hat{\pi}\}_s \left[ \int d\mathbf{v} e^{-\frac{\beta}{2}(\lambda_\theta(t) - \{\hat{\omega}\}_s)v^2 + \beta(\theta q(t)X + \{\hat{h}\}_s)v + \beta t f(u, v, X)} \right]^n \\ &= \lim_{n \rightarrow 0} \frac{1}{n} \ln \mathbb{E}_X \left[ 1 + n \sum_{s=0}^{\infty} \frac{\hat{\phi}^s e^{-\hat{\phi}}}{s!} \int \{d\hat{\pi}\}_s \ln \int d\mathbf{v} e^{-\frac{\beta}{2}(\lambda_\theta(t) - \{\hat{\omega}\}_s)v^2 + \beta(\theta q(t)X + \{\hat{h}\}_s)v + \beta t f(u, v, X)} \right] \\ &= \mathbb{E}_X \sum_{s=0}^{\infty} p_s^{(\hat{\phi})} \int \{d\hat{\pi}\}_s \ln \int d\mathbf{v} e^{-\frac{\beta}{2}(\lambda_\theta(t) - \{\hat{\omega}\}_s)v^2 + \beta(\theta q(t)X + \{\hat{h}\}_s)v + \beta t f(u, v, X)}, \end{aligned} \quad (A26)$$

where we have first expanded the exponential  $\exp(i\hat{\varphi}^*(\mathbf{v}))$  of the conjugate field in a Taylor series, then inserted the ansatz (A25d), and finally extracted the  $n \rightarrow 0$  behaviour. We introduced here the shorthands anticipated in the main text, namely  $\{d\hat{\pi}\}_s = \prod_{\ell=1}^s d\hat{\omega}_\ell d\hat{h}_\ell \pi(\hat{\omega}_\ell, \hat{h}_\ell)$  and  $\{x\}_s = \sum_{\ell=1}^s x_\ell$ . Note the appearance of the Poissonian degree distribution of average  $\hat{\phi}$

$$p_k^{(\hat{\phi})} = \frac{\hat{\phi}^k}{k!} e^{-\hat{\phi}}$$

corresponding to the degree distribution of an Erdős-Rényi graph of average degree  $\hat{\phi}$ . In the following, given a function  $f(k)$ , we will use the shorthand notation

$$\langle f(k) \rangle_{\hat{\phi}} := \sum_{k=0}^{\infty} f(k) \frac{\hat{\phi}^k}{k!} e^{-\hat{\phi}}.$$

The other terms in the action can be treated in a similar way, and we refer to [72] for the details of the calculation. The introduction of  $\pi$  and  $\hat{\pi}$  leads to a rewriting

$$\mathbb{E}_{\mathbf{A}}[(Z_\beta[\mathbf{A}; tF])^n] \approx e^{N\mathcal{S}_\beta[\pi, \hat{\pi}, \lambda_\theta(t), q(t); t, f]}, \quad (\text{A27})$$

where  $\mathcal{S}_\beta[\pi, \hat{\pi}, \lambda_\theta(t), q(t); t, f]$  is the action at the saddle point  $\mathcal{S}_\beta[\varphi^*, \hat{\varphi}^*, \psi^*, \hat{\psi}^*, \lambda^*(t); t, f]$  from Eq. (A13) with the ansatz in Eqs. (A25) inserted. In the  $n \rightarrow 0$  limit we get the expression

$$\begin{aligned} s_\beta[\pi, \hat{\pi}, q(t), \lambda_\theta(t); t] &:= \lim_{n \rightarrow 0} \frac{1}{n\beta} \mathcal{S}_\beta[\pi, \hat{\pi}, \lambda_\theta; t, f] = \frac{c}{2\beta} \int \mathbb{E}_W \left[ \ln \frac{\mathcal{Z}_\beta^{(2)}(h, \omega, h', \omega', W)}{\mathcal{Z}_\beta(\omega, h) \mathcal{Z}_\beta(\omega', h')} \right] d\pi(\omega, h) d\pi(\omega', h') \\ &\quad - \frac{\hat{\phi}}{\beta} \int \ln \frac{\mathcal{Z}_\beta(\omega - \hat{\omega}, h + \hat{h})}{\mathcal{Z}_\beta(\omega, h)} d\pi(\omega, h) d\hat{\pi}(\hat{\omega}, \hat{h}) - \frac{\theta}{2} q(t)^2 + \frac{1}{2} \lambda_\theta(t) + I_f[\hat{\pi}, q(t), \lambda_\theta(t); t], \end{aligned} \quad (\text{A28})$$

where we use the shorthands  $d\pi(\omega, h) = \pi(\omega, h) d\omega d\hbar$  and  $W$  is distributed as  $\varrho_W$ . We have also introduced

$$\mathcal{Z}_\beta^{(2)}(h, \omega, h', \omega', W) = \int d\mathbf{v} d\mathbf{v}' e^{-\frac{\beta}{2}\omega v^2 + \beta h v - \frac{\beta}{2}\omega' v'^2 + \beta h' v' + \beta W v v'} = \mathcal{Z}_\beta(\omega', h') \mathcal{Z}_\beta\left(\omega - \frac{W^2}{\omega'}, h + \frac{h' W}{\omega'}\right). \quad (\text{A29})$$

The quantity  $s_\beta[\pi, \hat{\pi}, q(t), \lambda_\theta(t); t]$  will allow for multiple computations. For example, if we invoke Eq. (12) we have

$$\mathbb{E}_{\mathbf{A}}[\lambda_{\text{top}}] = \lim_{\beta \rightarrow \infty} \frac{2}{\beta} \lim_{n \rightarrow 0} \frac{1}{n} \lim_{N \rightarrow \infty} \frac{1}{N} \ln \mathbb{E}_{\mathbf{A}}[Z_\beta^n(\mathbf{A})] = 2 \lim_{\beta \rightarrow +\infty} s_\beta(\pi, \hat{\pi}, q(t=0), \lambda_\theta(t=0); t=0)$$

for the average top eigenvalue, since  $Z_\beta(\mathbf{A})$  is obtained from  $Z_\beta[\mathbf{A}; tF]$  by setting  $t = 0$ . This case is tackled in the next subsection.

### 1. Saddle point equations for $\pi$ and $\hat{\pi}$ and average top eigenvalue

Setting  $t = 0$  in the above equations, and inserting the ansatz in Eqs. (A25) into Eq. (A21), upon extraction of the  $n \rightarrow 0$  limit at finite  $\beta$  we obtain the first one of the integral conditions linking  $q \equiv q(t=0)$  and  $\lambda_\theta \equiv \lambda_\theta(t=0)$ , namely

$$q = \mathbb{E}_X \left\langle \int \{d\hat{\pi}\}_k \frac{\{\hat{h}\}_k X + \theta q X^2}{\lambda_\theta - \{\hat{\omega}\}_k} \right\rangle_{\hat{\phi}}, \quad (\text{A30})$$

while inserting the ansatz into the saddle point equation (A22) we obtain

$$1 = \mathbb{E}_X \left\langle \int \{d\hat{\pi}\}_k \left[ \frac{1}{\beta(\lambda_\theta - \{\hat{\omega}\}_k)} + \left( \frac{\{\hat{h}\}_k + \theta q X}{\lambda_\theta - \{\hat{\omega}\}_k} \right)^2 \right] \right\rangle_{\hat{\phi}}. \quad (\text{A31})$$

Next, inserting the ansatz into the saddle-point equation for  $i\hat{\varphi}^*(\mathbf{v})$  in Eq. (A23), integrating over  $\mathbf{v}$  and extracting the  $n \rightarrow 0$  limit we get

$$\hat{\phi} \int d\hat{\pi}(\hat{\omega}, \hat{h}) \ln \mathcal{Z}_\beta(\hat{\omega}, \hat{h}) = c \int d\pi(\omega, h) \mathbb{E}_W \left[ \ln \mathcal{Z}_\beta\left(\frac{W^2}{\omega}, \frac{hW}{\omega}\right) \right], \quad (\text{A32})$$

and, crucially, we observe by inspection that the normalised joint distribution  $\hat{\pi}$

$$\hat{\pi}(\hat{\omega}, \hat{h}) = \int d\pi(\omega, h) \mathbb{E}_W \left[ \delta\left(\hat{\omega} - \frac{W^2}{\omega}\right) \delta\left(\hat{h} - \frac{hW}{\omega}\right) \right] \quad (\text{A33})$$

solves Eq. (A32), provided that  $\hat{\phi} = c$ . With this ansatz,  $p_k^{(\hat{\phi})}$  is precisely the Poisson distribution with average  $c$  corresponding to the starting graph topology in Eq. (A4) in the large  $N$  limit.

Similarly, let us insert the ansatz into the saddle point equation for  $\varphi^*(\mathbf{v})$  in Eq. (A24) and multiply by a test kernel  $K(\mathbf{v}) = \prod_{a=1}^n \frac{1}{Z_\beta(\omega', h')} \exp\left(-\beta \frac{\omega'}{2} v_a^2 + \beta h' v_a\right)$ . By integrating both sides over  $\mathbf{v}$  we obtain, upon extraction of the  $n \rightarrow 0$  limit,

$$\int d\pi \ln \frac{Z_\beta(\omega + \omega', h + h')}{Z_\beta(\omega, h) Z_\beta(\omega', h')} = \mathbb{E}_X \left\langle \left\langle \int \{d\hat{\pi}\}_{k-1} \ln \frac{Z_\beta(\lambda_\theta - \{\hat{\omega}\}_{k-1} + \omega', \theta q X + \{\hat{h}\}_{k-1} + h')}{Z_\beta(\lambda_\theta - \{\hat{\omega}\}_{k-1}, \theta X q + \{\hat{h}\}_{k-1}) Z_\beta(\omega', h')} \right\rangle \right\rangle_c. \quad (\text{A34})$$

Note that, given a function  $f(k)$ , we have denoted  $\frac{1}{c} \langle k f(k) \rangle_c \equiv \langle\langle f(k) \rangle\rangle_c$ , namely the average  $\langle\langle \bullet \rangle\rangle_c$  has to be intended with respect to *degree-corrected distribution* associated to a Poissonian distribution of mean  $c$ , as per Eq. (18) in the main text. As Eq. (A34) must hold for all values of the non-integrated variables  $\omega', h'$ , it can be translated into

$$\pi(\omega, h) = \mathbb{E}_X \left\langle \left\langle \int \{d\hat{\pi}\}_{k-1} \delta(\omega - (\lambda_\theta - \{\hat{\omega}\}_{k-1})) \delta(h - (\{\hat{h}\}_{k-1} + \theta q X)) \right\rangle \right\rangle_c, \quad (\text{A35})$$

which solves Eq. (A34). By inserting Eq. (A33) into the right hand side of Eq. (A35), and replacing the Poissonian degree distribution of average  $c$  with a *generic* degree distribution  $p_k$  with finite connectivity and bounded maximal degree via the anticipated recipe in Appendix B of [19], we obtain the *recursive distributional equation* (19a) in the main text — namely, an integral equation for the joint probability density function  $\pi(\omega, h)$  that governs how the  $\omega$  and  $h$  fields need to be distributed on the edges of an associated auxiliary graph whose weighted adjacency matrix is  $\mathbf{J}$  (see [72] for a more detailed explanation in the context of the cavity method). Equations with this structure appear in the mathematical literature on random graphs [25–28] and in statistical physics and inference [23, 24], and can be efficiently solved using a population dynamics algorithm [22] as described in Appendix C.

*a. Average top eigenvalue: exact expression from the action* Once the saddle point equation for  $\pi$  has been identified, we turn our attention to the explicit expression for  $\mathbb{E}[\lambda_{\text{top}}]$ . In previous results available in the literature on sparse symmetric matrix models solved via the same method, the Lagrange multiplier  $\lambda_\theta$  solving the Eqs. (19) was numerically observed to provide precisely this quantity [19]: this fact was later proved for the diluted Wishart model [21]. Below, we outline the proof within our setup. Let us start by observing that the leading  $\beta \rightarrow \infty$  term of the action  $s_\beta$  reads

$$\lim_{\beta \rightarrow +\infty} s_\beta[\pi, \hat{\pi}, q, \lambda_\theta; t = 0] = \frac{1}{2} \left( -\frac{c}{2} I_1[\pi] - c I_2[\pi] + 2\lambda_\theta - \theta q^2 \right), \quad (\text{A36})$$

where we have introduced [76]

$$I_1[\pi] := \int d\pi(\omega, h) d\pi(\omega', h') \mathbb{E}_W \left[ \frac{\left( h + \frac{h'W}{\omega'} \right)^2}{\omega - \frac{W^2}{\omega'}} - \frac{h^2}{\omega} \right], \quad (\text{A37})$$

$$I_2[\pi] := \int d\pi(\omega, h) d\pi(\omega', h') \mathbb{E}_W \left[ \left( \frac{h + \frac{W h'}{\omega'}}{\omega - \frac{W^2}{\omega'}} \right)^2 \frac{W^2}{\omega'} \right]. \quad (\text{A38})$$

From the top eigenvalue formula in Eq. (A30) we therefore obtain

$$\mathbb{E}_A[\lambda_{\text{top}}] = -\frac{c}{2} I_1[\pi] - c I_2[\pi] + 2\lambda_\theta - \theta q^2. \quad (\text{A39})$$

We will obtain a more compact expression by expanding the leading terms of the entropic term  $I_f[\hat{\pi}, q, \lambda_\theta; t = 0]$  (that effectively does not depend on  $f$ ) in the  $\beta \rightarrow \infty$  limit in two different ways, and recall that in the previous section we have obtained the condition  $\hat{\phi} = c$ . First, we write down the leading  $\beta \rightarrow \infty$  term

$$I_f[\hat{\pi}, q, \lambda_\theta; t = 0] = \frac{1}{\beta} \mathbb{E}_X \left\langle \int \{d\hat{\pi}\}_k \ln Z_\beta \left( \lambda_\theta - \{\hat{\omega}\}_k, \{\hat{h}\}_k + \theta q X \right) \right\rangle_c \xrightarrow{\beta \rightarrow \infty} \frac{1}{2} \mathbb{E}_X \left\langle \int \{d\hat{\pi}\}_k \frac{(\{\hat{h}\}_k + \theta q X)^2}{\lambda_\theta - \{\hat{\omega}\}_k} \right\rangle_c. \quad (\text{A40})$$

We now proceed in two ways. First, we divide and multiply by the denominator to simplify the first term using the normalisation in Eq. (A31) to obtain

$$\lim_{\beta \rightarrow +\infty} I_f[\hat{\pi}, q, \lambda_\theta; t = 0] = \frac{1}{2} \lambda_\theta - \frac{1}{2} \mathbb{E}_X \left\langle \int \{d\hat{\pi}\}_k \left( \frac{\{\hat{h}\}_k + \theta q X}{\lambda_\theta - \{\hat{\omega}\}_k} \right)^2 \{\hat{\omega}\}_k \right\rangle_c \quad (\text{A41})$$

$$\begin{aligned}
&= \frac{1}{2} \lambda_\theta - \frac{c}{2} \mathbb{E}_X \int d\hat{\pi}(\hat{\omega}, \hat{h}) \hat{\omega} \left\langle \left\langle \int \{d\hat{\pi}\}_{k-1} \left( \frac{\{\hat{h}\}_{k-1} + \hat{h} + \theta q X}{\lambda_\theta - \{\hat{\omega}\}_{s-1} - \hat{\omega}} \right)^2 \right\rangle \right\rangle_c \\
&\stackrel{\text{Eq. (A35)}}{=} \frac{1}{2} \lambda_\theta - \frac{c}{2} \int d\hat{\pi} d\pi \left( \frac{h + \hat{h}}{\omega - \hat{\omega}} \right)^2 \hat{\omega} \\
&\stackrel{\text{Eq. (A33)}}{=} \frac{1}{2} \lambda_\theta - \frac{c}{2} \int d\pi(\omega, h) d\pi(\omega', h') \mathbb{E}_W \left[ \left( \frac{h + \frac{Wh'}{\omega'}}{\omega - \frac{W^2}{\omega'}} \right)^2 \frac{W^2}{\omega'} \right] \\
&= \frac{\lambda_\theta - cI_2[\pi]}{2} , \tag{A42}
\end{aligned}$$

where in the third step we have inserted the identity

$$1 = \int d\omega d h \delta(\hat{\omega} - (\lambda_\theta - \{\hat{\omega}\}_{s-1})) \delta(\hat{h} - (\lambda_\theta - (\{\hat{h}\}_{s-1} + \theta q X)))$$

and used Eq. (A35), whereas in the last step we have used Eq. (A33) and recognised  $I_2[\pi]$  defined in Eq. (A38).

The second way to proceed from Eq. (A40) is to expand one of the factors in the numerator, writing

$$\lim_{\beta \rightarrow +\infty} I_f[\hat{\pi}, q, \lambda_\theta; t = 0] = \frac{1}{2} \mathbb{E}_X \left\langle \int \{d\hat{\pi}\}_k \frac{\{\hat{h}\}_k + \theta q X}{\lambda_\theta - \{\hat{\omega}\}_k} \{\hat{h}\}_k \right\rangle_c + \frac{\theta q}{2} \mathbb{E}_X \left\langle \int \{d\hat{\pi}\}_k \frac{\{\hat{h}\}_k X + \theta q X^2}{\lambda_\theta - \{\hat{\omega}\}_k} \right\rangle_c \tag{A43}$$

$$\begin{aligned}
&= \frac{c}{2} \int d\pi(\omega, h) d\pi(\omega', h') \mathbb{E}_W \left[ \frac{h + \frac{Wh'}{\omega'}}{\omega - \frac{W^2}{\omega'}} \frac{Wh'}{\omega'} \right] + \frac{\theta q^2}{2} \\
&\equiv \frac{cI_1[\pi] + 2\theta q^2}{4} , \tag{A44}
\end{aligned}$$

where for the first term we proceeded analogously to the derivation in Eq. (A42), and for the second term we used the expression for  $q$  in Eq. (A30). Next, we have noted [21] that

$$\frac{h + \frac{h'W}{\omega'}}{\omega - \frac{W^2}{\omega'}} \frac{h'W}{\omega'} = \frac{1}{2} \left[ \left( \frac{\left( h + \frac{h'W}{\omega'} \right)^2}{\omega - \frac{W^2}{\omega'}} - \frac{h^2}{\omega} \right) - \frac{W^2}{\omega\omega' - W^2} \left( \frac{h^2}{\omega} - \frac{h'^2}{\omega'} \right) \right] , \tag{A45}$$

and integrated both sides with respect to  $d\pi(\omega, h)$  and  $d\hat{\pi}(\hat{\omega}, \hat{h})$ . The double integral of the second term on the R.H.S. of the above equation vanishes due to symmetry of the variables  $h \leftrightarrow h', \omega \leftrightarrow \omega'$ , thus reducing Eq. (A45) to  $\frac{1}{2}I_1[\pi]$ , defined in Eq. (A37). Finally, by equating Eq. (A42) with Eq. (A44), we write  $-\frac{c}{2}I_1[\pi] - cI_2[\pi] = -\lambda_\theta + \theta q^2$  which, inserted back into Eq. (A39), gives the result

$$\mathbb{E}_{\mathbf{A}}[\lambda_{\text{top}}] = \lambda_\theta . \tag{A46}$$

## 2. Top eigenvector component density and overlap

In this section, we show a detailed derivation of quantities of the form in Eq. (14), namely

$$\lim_{N \rightarrow +\infty} \mathbb{E}_{\mathbf{A}}[F(u, v_{\text{top}}, x)] = \lim_{\beta \rightarrow +\infty} \lim_{n \rightarrow 0} \lim_{N \rightarrow +\infty} \frac{1}{\beta n N} \frac{\partial}{\partial t} \ln \mathbb{E}_{\mathbf{A}}[(Z_\beta[\mathbf{A}; tF])^n] \Big|_{t=0} \tag{A47}$$

$$= \lim_{\beta \rightarrow +\infty} \lim_{n \rightarrow 0} \frac{1}{\beta n} \frac{\partial}{\partial t} \mathcal{S}_\beta[\varphi^*, \hat{\varphi}^*, \psi^*, \hat{\psi}^*, \lambda^*(t); t, f] \Big|_{t=0} , \tag{A48}$$

where the action  $\mathcal{S}_\beta$  is given in Eq. (A14). By the chain rule,

$$\frac{\partial \mathcal{S}_\beta}{\partial t} = \frac{\partial \mathcal{S}_\beta}{\partial \varphi} \Big|_* \frac{\partial \varphi^*}{\partial t} + \frac{\partial \mathcal{S}_\beta}{\partial \hat{\varphi}} \Big|_* \frac{\partial \hat{\varphi}^*}{\partial t} + \frac{\partial \mathcal{S}_\beta}{\partial \psi} \Big|_* \frac{\partial \psi^*}{\partial t} + \frac{\partial \mathcal{S}_\beta}{\partial \hat{\psi}} \Big|_* \frac{\partial \hat{\psi}^*}{\partial t} + \frac{\partial \mathcal{S}_\beta}{\partial \lambda} \Big|_* \frac{\partial \lambda^*}{\partial t} + \frac{\partial \mathcal{S}_\beta}{\partial t} , \tag{A49}$$

where all the starred terms vanish because the action is stationary at the saddle point. Therefore, only the explicit dependence on  $t$  matters in the entropic term which leads us to the expression for the observable

$$\lim_{N \rightarrow +\infty} \mathbb{E}_{\mathbf{A}}[F(u, v_{\text{top}}, x)] \equiv \lim_{\beta \rightarrow +\infty} \frac{\partial}{\partial t} I_f[\hat{\pi}, q, \lambda_\theta; t] \Big|_{t=0}, \quad (\text{A50})$$

provided the observable is of the form  $F(u, v, x) = \frac{1}{N} \sum_i f(u, v_i, x_i)$  as in Eq. (A2) and  $I_f$  is defined in Eq. (A26). The final result thus reads as

$$\lim_{N \rightarrow +\infty} \mathbb{E}_{\mathbf{A}}[F(u, v_{\text{top}}, x)] = \lim_{\beta \rightarrow +\infty} \mathbb{E}_X \left\langle \int \{d\hat{\pi}\}_k \frac{\int dv f(u, v, X) e^{-\frac{\beta}{2}(\lambda_\theta - \{\hat{\omega}\}_k)v^2 + \beta(\{\hat{h}\}_k + \theta q X)v}}{\mathcal{Z}_\beta(\lambda_\theta - \{\hat{\omega}\}_k, \{\hat{h}\}_k + \theta q X)} \right\rangle, \quad (\text{A51})$$

where we have replaced the Poissonian degree distribution with a generic degree distribution  $p_k$  as justified at the end of Appendix. A 1.

a. *Density of the entries of  $v_{\text{top}}$*  In this section, we choose

$$F(u, v_{\text{top}}, x) \mapsto F_{\text{top}}(u, v_{\text{top}}) := \frac{1}{N} \sum_{i=1}^N \delta(u - v_{1,i}),$$

which corresponds to  $f(u, v, X) = \delta(u - vg(X))$  with  $g(X) = 1$ . Inserting this into Eq. (A51), we get

$$\begin{aligned} \varrho_{\text{top}}(u) &= \lim_{N \rightarrow +\infty} \mathbb{E}_{\mathbf{A}}[F_{\text{top}}(u, v_{\text{top}})] = \mathbb{E}_X \left\langle \int \{d\hat{\pi}\}_k \delta \left( u - \frac{\{\hat{h}\}_k + \theta q X}{\lambda_\theta - \{\hat{\omega}\}_k} \right) \right\rangle \\ &= \mathbb{E}_X \left\langle \int \{d\pi\}_k \{d\varrho_W\}_k \delta \left( u - \frac{\{\frac{W^h}{\omega}\}_k + \theta q X}{\lambda_\theta - \{\frac{W^2}{\omega}\}_k} \right) \right\rangle, \end{aligned} \quad (\text{A52})$$

where in the last step we use the definition of  $\hat{\pi}$  in Eq. (A33). Setting  $\theta = 0$  or  $\varrho_x(x) = \delta(x)$  indeed recovers the top eigenvector density for the unspiked model analysed in [19].

b. *Overlap between  $v_{\text{top}}$  and  $x$*  In this section, we present the calculation to compute the overlap between the top eigenvector and signal vector. We pick

$$F(u, v_{\text{top}}, x) \mapsto F_{\text{ov}}(u, v_{\text{top}}, x) := \frac{1}{N} \sum_{i=1}^N \delta(u - x_i v_{1,i}) \quad (\text{A53})$$

which corresponds to the choice  $f(u, v, X) = \delta(u - vg(X))$  with  $g(X) = X$ . Inserting this into Eq. (A51), we obtain

$$\begin{aligned} \varrho_{\text{ov}}(u) &= \lim_{N \rightarrow +\infty} \mathbb{E}_{\mathbf{A}}[F_{\text{ov}}(u, v_{\text{top}}, x)] = \lim_{\beta \rightarrow +\infty} \mathbb{E}_X \left\langle \int \{d\hat{\pi}\}_k \frac{\int dv \delta(u - xv) e^{-\frac{\beta}{2}(\lambda_\theta - \{\hat{\omega}\}_k)v^2 + \beta(\{\hat{h}\}_k + \theta q X)v}}{\mathcal{Z}_\beta(\lambda_\theta - \{\hat{\omega}\}_k, \{\hat{h}\}_k + \theta q X)} \right\rangle \\ &= \mathbb{E}_X \left\langle \int \{d\pi\}_k \{d\varrho_W\}_k \delta \left( u - \frac{X \{\frac{W^h}{\omega}\}_k + \theta q X^2}{\lambda_\theta - \{\frac{W^2}{\omega}\}_k} \right) \right\rangle. \end{aligned} \quad (\text{A54})$$

Then, we express the average overlap as

$$\lim_{N \rightarrow \infty} \mathbb{E}_{\mathbf{A}} \left[ \frac{\langle x, v_{\text{top}} \rangle}{N} \right] = \lim_{N \rightarrow \infty} \int u \varrho_{\text{ov}}(u) du = \mathbb{E}_X \left\langle \int \{d\pi\}_k \{d\varrho_W\}_k \frac{X \{\frac{W^h}{\omega}\}_k + \theta q X^2}{\lambda_\theta - \{\frac{W^2}{\omega}\}_k} \right\rangle. \quad (\text{A55})$$

Note that this is the same expression as Eq. (A30) and we thus identify the auxiliary variable  $q$  as the typical value of the overlap. Similarly, the average squared overlap is

$$\lim_{N \rightarrow \infty} \mathbb{E}_{\mathbf{A}} \left[ \frac{\langle x, v_{\text{top}} \rangle^2}{N^2} \right] = \lim_{N \rightarrow \infty} \int u^2 \varrho_{\text{ov}}(u) du = \mathbb{E}_X \left\langle \int \{d\pi\}_k \{d\varrho_W\}_k \left( \frac{X \{\frac{W^h}{\omega}\}_k + \theta q X^2}{\lambda_\theta - \{\frac{W^2}{\omega}\}_k} \right)^2 \right\rangle. \quad (\text{A56})$$

## Appendix B: Explicit results for the threshold, top eigenvalue and squared overlap in the ER and RR models

In this Appendix, we outline the derivation of the critical threshold  $\theta_{\text{crit}}$  in the notable cases discussed in the

main text. We start by defining

$$m(\lambda_\theta) := \int dh d\omega \frac{\pi(\omega, h)}{\omega}. \quad (\text{B1})$$

Let  $W \sim \varrho_W$  be a random variable. By Eq. (19a) we obtain

$$\begin{aligned} m(\lambda_\theta) &= \left\langle \left\langle \int \{d\pi\}_{k-1} \{d\varrho_W\}_{k-1} \frac{1}{\lambda_\theta - \left\{ \frac{W^2}{\omega} \right\}_{k-1}} \right\rangle \right\rangle \\ &= \frac{1}{\lambda_\theta} \left\langle \left\langle \sum_{p=0}^{\infty} \left( \frac{(k-1)\mathbb{E}_W[W^2]m(\lambda_\theta)}{\lambda_\theta} \right)^p \right\rangle \right\rangle \\ &= \left\langle \left\langle \frac{1}{\lambda_\theta - (k-1)\mathbb{E}_W[W^2]m(\lambda_\theta)} \right\rangle \right\rangle, \end{aligned} \quad (\text{B2})$$

where we have applied a geometric series expansion, and we recall that  $\langle\langle \bullet \rangle\rangle$  is the average of a function of  $k$  over  $r_k \propto kp_k$ , degree-corrected distribution of  $p_k$  in Eq. (18).

### 1. Poissonian noise

Let us first consider the (truncated) Poissonian noise case, namely a noise matrix generated by using  $\varrho_W(W) = \delta(W-1)$  and

$$p_k = \frac{\bar{c}^k}{\Gamma k!}, \quad \Gamma := \sum_{k=0}^{k_{\max}} \frac{\bar{c}^k}{k!}.$$

We will present here the derivation of Result IV.1. Consider Eq. (26) for  $Q(\lambda_\theta)$  that determines the critical value  $\theta_{\text{crit}}$ ,

$$Q(\lambda_\theta) = \left\langle \int \{d\pi\}_k \{d\varrho_W\}_k \frac{1}{\lambda_\theta - \left\{ \frac{W^2}{\omega} \right\}_k} \right\rangle, \quad (\text{B3})$$

where the average  $\langle\bullet\rangle$  is taken as usual w.r.t.  $p_k$ . We now wish to re-express the right hand side of (B3) in terms of  $m(\lambda_\theta)$ , as defined in Eq. (B1). To do so, we express  $m(\lambda_\theta)$  in a different way. Multiplying both sides of Eq. (19a) by  $1/\omega$  and integrating, we obtain

$$\begin{aligned} m(\lambda_\theta) &= \\ &= \sum_{k=1}^{k_{\max}} \frac{\bar{c}^k}{(k-1)!c\Gamma} \int \{d\pi\}_{k-1} \{d\varrho_W\}_{k-1} \frac{1}{\lambda_\theta - \left\{ \frac{W^2}{\omega} \right\}_{k-1}} \\ &= \sum_{k=0}^{k_{\max}-1} \frac{\bar{c}}{c} \frac{\bar{c}^k}{\Gamma k!} \int \{d\pi\}_k \{d\varrho_W\}_k \frac{1}{\lambda_\theta - \left\{ \frac{W^2}{\omega} \right\}_k} \\ &= \frac{\bar{c}}{c} [\tilde{Q}(\lambda_\theta) - R(\theta, k_{\max})], \end{aligned}$$

where the correction term  $R(\theta, k_{\max})$  takes care of the mismatch between the upper limits of the sums. It reads

$$\begin{aligned} R(\theta, k_{\max}) &:= \\ &= \frac{\bar{c}^{k_{\max}}}{\Gamma k_{\max}!} \int \{d\pi\}_{k_{\max}} \{d\varrho_W\}_{k_{\max}} \frac{1}{\lambda_\theta - \left\{ \frac{W^2}{\omega} \right\}_{k_{\max}}} \\ &= \frac{\bar{c}^{k_{\max}}}{\Gamma k_{\max}!} \frac{1}{\lambda_\theta - k_{\max} \mathbb{E}_W[W^2]m(\lambda_\theta)}, \end{aligned}$$

where we have again expanded and resummed the geometric series. Summarising, we get

$$\tilde{Q}(\lambda_\theta) = \frac{c}{\bar{c}} m(\lambda_\theta) + \frac{\bar{c}^{k_{\max}}}{\Gamma k_{\max}!} \frac{1}{\lambda_\theta - k_{\max} \mathbb{E}_W[W^2]m(\lambda_\theta)}, \quad (\text{B4})$$

where  $m(\lambda_\theta)$  satisfies Eq. (B2). The result for  $\theta_{\text{crit}}$  in (30) readily follows.

For a set value of  $\theta > \theta_{\text{crit}}$ , the top eigenvalue associated with the signal overtakes the noise structural one,  $\lambda_\theta > \lambda_{\theta=0}$ . Recalling the condition in Eq. (27), we obtain the value of the top eigenvalue associated with the signal as

$$\lambda_\theta = \tilde{Q}^{-1} \left( \frac{1}{\theta \sigma_x^2} \right), \quad (\text{B5})$$

which can be easily determined by numerically solving Eq. (B4) using Eq. (B2). To compute the squared overlap, consider the partition function defined in Eq. (9)

$$Z_\beta(\mathbf{A}) = \int d\mathbf{v} \exp \left[ \frac{\beta}{2} \langle \mathbf{v}, \mathbf{J} \mathbf{v} \rangle + \frac{\beta \theta}{N} \langle \mathbf{x}, \mathbf{v} \rangle^2 \right] \delta(\|\mathbf{v}\|^2 - N). \quad (\text{B6})$$

For  $\theta > \theta_{\text{crit}}$ , by taking the derivative of its logarithm with respect to the signal strength parameter gives us in the large  $\beta$  limit we get

$$\frac{\partial \mathbb{E}_\mathbf{A}[\lambda_{\text{top}}]}{\partial \theta} = \lim_{\beta \rightarrow \infty} \frac{2}{N} \frac{\partial}{\partial \theta} \mathbb{E}_\mathbf{A} \ln Z_\beta(\mathbf{A}) = \mathbb{E}_\mathbf{A} \left[ \frac{\langle \mathbf{x}, \mathbf{v}_{\text{top}} \rangle^2}{N^2} \right], \quad (\text{B7})$$

where we recalled the Courant–Fischer–Weyl formulation in Section II A. Using Eq. (B5) we obtain the value of the squared overlap for  $\theta > \theta_{\text{crit}}$  as

$$\mathbb{E}_\mathbf{A} \left[ \frac{\langle \mathbf{x}, \mathbf{v}_{\text{top}} \rangle^2}{N^2} \right] = -\frac{1}{\sigma_x^2 \theta^2 \tilde{Q}'(\lambda_\theta)}. \quad (\text{B8})$$

### 2. Random regular noise

An analytic expression for the critical threshold, top eigenvalue and squared overlap can be also obtained in the RR setup in Eq. (7). In this case, each row of the noise matrix  $\mathbf{J}$  has a exactly  $c$  nonzero elements. We set for simplicity  $\varrho_W(W) = \delta(W-1)$  so that the RDE for  $\pi(\omega, h)$  in Eq. (19a) reads as

$$\begin{aligned} \pi(\omega, h) &= \\ &= \mathbb{E}_X \int \{d\pi\}_{c-1} \delta \left( \omega - \lambda_\theta + \left\{ \frac{1}{\omega} \right\}_{c-1} \right) \delta \left( h - \left\{ \frac{h}{\omega} \right\}_{c-1} - \theta q X \right) \end{aligned} \quad (\text{B9})$$

and the adopted ansatz therein becomes  $\pi(\omega, h) = \delta(\omega - \bar{\omega}) \mathbb{E}_X \delta(h - \bar{h}(X))$ , where  $X \sim \varrho_x$  has zero mean and variance  $\sigma_x^2$ . First, notice that the ansatz gives us the

recursive equation for  $\bar{\omega} = \lambda_\theta - \sum_{\ell=1}^{c-1} \frac{1}{\omega} = \lambda_\theta - (c-1) \frac{1}{\bar{\omega}}$ . Solving for  $\bar{\omega}$ ,

$$\frac{1}{\bar{\omega}} = \frac{\lambda_\theta - \sqrt{\lambda_\theta^2 - 4(c-1)}}{2(c-1)} . \quad (\text{B10})$$

Note that the RHS is exactly the Kesten-McKay Stieltjes transform [77, 78] for a  $c$ -regular random graph. The reduced expressions of the normalisation and  $q$  are

$$1 = \mathbb{E}_X \left( \frac{\{\frac{h}{\omega}\}_c + \theta q X}{\lambda_\theta - \{\frac{1}{\omega}\}_c} \right)^2 \text{ and } q = \mathbb{E}_X \left[ \frac{X \{\frac{h}{\omega}\}_c + \theta q X^2}{\lambda_\theta - \{\frac{1}{\omega}\}_c} \right] , \quad (\text{B11})$$

respectively. Recall Eq. (26)

$$Q(\lambda_\theta) := \left\langle \int \{d\pi\}_k \{d\varrho_W\}_k \frac{1}{\lambda_\theta - \{\frac{W^2}{\omega}\}_k} \right\rangle , \quad (\text{B12})$$

which, upon the insertion of the RRG ansatz  $\pi(\omega, h)$ , gives  $Q(\lambda_\theta) = (\lambda_\theta - \frac{c}{\bar{\omega}})^{-1}$ . Also, recall that for  $q \neq 0$  Eq. (27) requires  $\theta\sigma_x^2 Q(\lambda_\theta) = 1$ . Then, the top eigenvalue associated with the signal that detaches from the bulk can be expressed as  $\lambda_\theta = c\bar{\omega}^{-1} + \theta\sigma_x^2$ . Finally, we use Eq. (B10) to obtain the explicit expression

$$\lambda_\theta = \frac{c}{2} \sqrt{\theta^2\sigma_x^4 + 4} - \frac{c-2}{2} \theta\sigma_x^2 , \quad (\text{B13})$$

which is the value of the eigenvalue associated with the spike once it detaches from the bulk. Recall that, in the thermodynamical limit, the spectrum of the adjacency matrix of a random regular graph with connectivity  $c$  has bulk edges at  $\pm 2\sqrt{c-1}$  and the structural top eigenvalue is  $\lambda_{\theta=0} = c$ . For a treatment of elementary spectral properties of graph adjacency matrices, see [79].

Using the previous facts, two thresholds in  $\theta$  are derived for the eigenvalue associated with the spike. The first threshold  $\theta_b$  corresponds to the value of the signal-to-noise ratio at which  $\lambda_\theta$  detaches from the bulk, i.e., where  $\lambda_{\theta=\theta_b} = 2\sqrt{c-1}$ , which gives the condition

$$\theta_b = \frac{c-2}{\sigma_x^2 \sqrt{c-1}} . \quad (\text{B14})$$

The second threshold  $\theta_{\text{crit}}$  corresponds to the condition  $\lambda_{\theta=0} = \lambda_{\theta=\theta_{\text{crit}}}$  expressing that  $\lambda_\theta$  overtakes the top structural eigenvalue  $\lambda_{\theta=0}$ , giving

$$\theta_{\text{crit}} = \frac{c(c-2)}{\sigma_x^2(c-1)} . \quad (\text{B15})$$

Simply inverting Eq. (B14), we obtain the value of  $c$  at which, for a given spike strength  $\theta$  and variance  $\sigma_x^2$ , the eigenvalue associated with the spike gets buried in the bulk

$$c_b = \frac{1}{4} \left( \theta\sigma_x^2 + \sqrt{(\theta\sigma_x^2)^2 + 4} \right)^2 + 1 , \quad (\text{B16})$$

whereas inverting Eq. (B15), we can determine the value of  $c$  at which the structural eigenvalue takes over the one associated with the spike, namely

$$c_{\text{crit}} = \frac{1}{2} \left( \theta\sigma_x^2 + \sqrt{(\theta\sigma_x^2)^2 + 4} \right) + 1 . \quad (\text{B17})$$

From the formula for the top eigenvalue, as outlined in Eq. (B7), we obtain the value of the squared overlap for  $\theta > \theta_{\text{crit}}$  from Eq. (B13)

$$\mathbb{E}_{\mathbf{A}} \left[ \frac{\langle \mathbf{x}, \mathbf{v}_{\text{top}} \rangle^2}{N^2} \right] = \frac{c\theta\sigma_x^4}{2\sqrt{(\theta\sigma_x^2)^2 + 4}} - \frac{(c-2)\sigma_x^2}{2} . \quad (\text{B18})$$

### 3. Large connectivity limit

In this section, we follow [19, 72] to determine the large connectivity limit  $c = \langle k \rangle \rightarrow \infty$  of our results for sparse matrices. We impose the condition  $\frac{\langle k^2 \rangle - \langle k \rangle^2}{\langle k \rangle^2} \rightarrow 0$  (i.e., the distribution concentrates around  $c = \langle k \rangle$  in this limit) and rescale the weights in  $\mathbf{W}$  to be of the form  $W_{ij} = \frac{1}{c} Z_{ij}$ . Let us also assume the signal distribution to be zero-centered with variance  $\sigma_x^2$ . In this limit and with the introduced assumptions, we expect to recover the well known BBP-like transition value  $\theta_{\text{crit}} = \frac{1}{\sigma_x^2}$  for the spiked (real) Wigner matrix ensemble [9–11]. In this model, for  $\theta > \theta_{\text{crit}} = \frac{1}{\sigma_x^2}$ , the top eigenvalue is  $\lambda_\theta = \sigma_x^2\theta + \frac{1}{\sigma_x^2\theta}$  and the squared overlap between the signal and the top eigenvector is  $\sigma_x^2 - (\theta\sigma_x)^{-2}$ .

In our setup, the transition value is given in Eq. (25)

$$\frac{1}{\theta_{\text{crit}}} = \sigma_x^2 \left\langle \int \{d\pi\}_k \{d\varrho_W\}_k \frac{1}{\lambda_{\theta=0} - \{\frac{W^2}{\omega}\}_k} \right\rangle . \quad (\text{B19})$$

In what follows, we shall be looking for an ansatz for the density  $\pi(\omega, h)$  as  $\langle k \rangle \rightarrow \infty$ . First, consider the argument of the first  $\delta$ -function on the R.H.S of Eq. (19a), which expresses the following identity in distribution,

$$\omega \stackrel{d}{=} \lambda_{\theta=0} - \frac{1}{c} \sum_{\ell=1}^{k-1} \frac{Z_\ell^2}{\omega_\ell} , \quad (\text{B20})$$

where  $k$  is randomly distributed as  $p_k$  and  $Z_\ell$  is a set of  $k-1$  rescaled bond weights. Given our assumptions and the concentration of  $k$  around  $c$ , by the Law of Large Numbers (LLN) as  $\langle k \rangle \rightarrow \infty$ , we have a concentration phenomenon leading to a deterministic value for  $\omega$ , which we denote  $\bar{\omega}$  and satisfies

$$\bar{\omega} = \lambda_{\theta=0} - \frac{\mathbb{E}_Z[Z^2]}{\bar{\omega}} . \quad (\text{B21})$$

Specialising for simplicity to  $\mathbb{E}_Z[Z] = 0$  and  $\mathbb{E}_Z[Z^2] = 1$ , the spectral density of  $\mathbf{J}$  is known to converge, as  $c \rightarrow \infty$ , to the Wigner semicircle law  $\varrho(\lambda) = \frac{1}{2\pi} \sqrt{4 - \lambda^2}$  with the right bulk edge at  $\lambda_{\theta=0} = 2$ . Inserting  $\lambda_{\theta=0} = 2$

and  $\mathbb{E}_Z[Z^2] = 1$  into the recursion for  $\bar{\omega}$  in Eq. (B21) we obtain  $\bar{\omega} = 1$ . We introduce therefore the ansatz  $\pi(\omega, h) = \delta(\omega - 1)\pi_h(h)$ , where  $\pi_h$  is the density of the  $\{h_\ell\}$  variables. Note, however, that  $\pi_h$  is irrelevant for the calculation of  $\theta_{\text{crit}}$  as  $\{h_\ell\}$  do not appear in Eq. (B19). Inserting  $\lambda_{\theta=0} = 2$  and the ansatz  $\pi(\omega, h) = \delta(\omega - 1)\pi_h(h)$  into Eq. (B19) we finally obtain the anticipated value

$$\theta_{\text{crit}} = \frac{1}{\sigma_x^2} \quad (\text{B22})$$

in the large connectivity limit.

For  $\theta > \theta_{\text{crit}}$  where the overlap is nonzero, the condition in Eq. (19c) (as  $q \neq 0$ ) gives in the large connectivity limit

$$\theta\sigma_x^2 = \lambda_\theta - \frac{1}{\bar{\omega}} = \bar{\omega} \quad (\text{B23})$$

where the large- $c$  limit of the first  $\delta$ -function on the R.H.S of Eq. (19a) (of the form as Eq. (B21) with  $\lambda_\theta$ ) has been used. This leads to

$$\lambda_\theta = \theta\sigma_x^2 + \frac{1}{\theta\sigma_x^2}. \quad (\text{B24})$$

Finally, the squared overlap is given

$$\mathbb{E}_A \left[ \frac{\langle x, v_{\text{top}} \rangle^2}{N^2} \right] = \frac{\partial \lambda_\theta}{\partial \theta} = \sigma_x^2 - \frac{1}{\theta^2 \sigma_x^2}, \quad (\text{B25})$$

once again recovering all relevant values in the spiked real Wigner case [9–11, 36].

### Appendix C: Spiked population dynamics

In this Appendix, we describe the implementation of the population dynamics algorithm (PDA) [22] adopted to efficiently determine the joint probability density  $\pi(\omega, h)$  in Eq. (19). This algorithm is outlined for  $\theta > \theta_{\text{crit}}$  (otherwise we are in the  $\theta = 0$  case studied in [19]).

The joint probability density function  $\pi(\omega, h)$  that solves Eq. (19a) is represented by a set of  $N_p$  pairs  $\mathcal{P} = \{(\omega_i, h_i)\}_{i=1}^{N_p}$ , initialised using a random uniform distribution on [5, 20] for  $\omega$  and [0, 10] for  $h$ . For a given set of parameters  $(q_{\text{init}}, \lambda_{\theta, \text{init}}, \theta)$  (we usually initialise  $q_{\text{init}} = 0.5$ ,  $\lambda_{\theta, \text{init}} = 10$ ) we perform the following steps:

1. Sample an integer  $k$  from  $r_k \propto kp_k$ .
2. Select at random  $k - 1$  pairs  $\{(\omega_\ell, h_\ell)\}_{\ell=1}^{k-1}$  from  $\mathcal{P}$ .
3. Sample  $k - 1$  values  $W_\ell$  with density  $\varrho_W$  and a value  $x \sim \varrho_x$ .

4. Compute a new pair  $(\omega_{\text{new}}, h_{\text{new}})$  as

$$\left( \lambda_{\theta, \text{init}} - \left\{ \frac{w^2}{\omega} \right\}_{k-1}, \left\{ \frac{hW}{\omega} \right\}_{k-1} + \theta q_{\text{init}} x \right)$$

as prescribed by Eq. (19a).

5. Replace a randomly selected pair in  $\mathcal{P}$  with  $(\omega_{\text{new}}, h_{\text{new}})$ .

6. Monitor four moments of the population for a set number of steps of the algorithm. Once they plateau,  $\mathcal{P}$  has reached equilibrium and the process ends, otherwise return to (1).

Once the population  $\mathcal{P}$  has reached equilibrium, we check the conditions that the population must satisfy. Compute the constants

$$\alpha_1 = \mathbb{E}_X \left\langle \int \{d\pi\}_k \{d\varrho_W\}_k \left( \frac{\{\frac{hW}{\omega}\}_k + \theta q X}{\lambda_\theta - \{\frac{W^2}{\omega}\}_k} \right)^2 \right\rangle$$

that checks Eq. (19b) and

$$\alpha_2 = \mathbb{E}_X \left\langle \int \{d\pi\}_k \{d\varrho_W\}_k \frac{X^2}{\lambda_\theta - \{\frac{W^2}{\omega}\}_k} \right\rangle$$

that checks Eq. (19c) (we know  $q \neq 0$  so we divide that equation by  $q$  on both sides). If, within some pre-fixed tolerance,  $\alpha_1 = 1$  and  $\alpha_2 = 1$  for an equilibrated population  $\mathcal{P}$ , we have obtained the population of interest that satisfies Eqs. (19a), (19b) and (19c).

Otherwise, if  $\alpha_1 \neq 1$  and  $\alpha_2 \neq 1$ , instead of searching over a grid  $(q, \lambda_\theta)$ , we perform rescaling steps informed by  $\alpha_1, \alpha_2$  that considerably speed up convergence to the desirable values. Rescale  $q_{\text{new}} = \frac{1}{\sqrt{\alpha}} q_{\text{init}} \mapsto q_{\text{init}}$  and  $\lambda_{\theta, \text{new}} = \alpha_2 \lambda_{\theta, \text{init}} \mapsto \lambda_{\theta, \text{init}}$  and repeat the above PDA steps (1–6) with parameters  $(q_{\text{init}} = q_{\text{new}}, \lambda_{\theta, \text{init}} = \lambda_{\theta, \text{new}}, \theta)$ . Upon convergence, if  $\alpha_1 \neq 1$  and  $\alpha_2 \neq 1$ , rescale  $q_{\text{new}}$  and  $\lambda_{\theta, \text{new}}$  and repeat the PDA steps (1–6) until we have obtained  $\alpha_1 = 1$  and  $\alpha_2 = 1$  (up to a suitable tolerance threshold).

Note, however, that in the settings of interest we have obtained  $\lambda_{\theta, \text{init}}$  and  $q_{\text{init}}$  explicitly. We use them as input parameters  $(q, \lambda_\theta, \theta)$ : for the truncated Poissonian degree distribution in Result IV.1, we use Eq. (31) to get  $\lambda_\theta$  and Eq. (32) to get  $q$ , and for random regular in Result IV.2 we use Eq. (35) for  $\lambda_\theta$  and Eq. (36) for  $q$ . Once these values are obtained, we perform one sweep of the PD algorithm (steps 1–6) to obtain the equilibrium population  $\mathcal{P}$  and use it to compute relevant observables.

[1] Ian T. Jolliffe. *Principal Component Analysis*. Springer Series in Statistics. Springer-Verlag, New York, 2002.

[2] Emmanuel J. Candès, Xiaodong Li, Yi Ma, and John

Wright. Robust principal component analysis? *J. ACM*, 58(3), 2011.

[3] Paul Holland, Kathryn B. Laskey, and Samuel Leinhardt. Stochastic blockmodels: First steps. *Social Networks*, 5:109–137, 1983.

[4] Emmanuel Abbe. Community detection and stochastic block models: Recent developments. *Journal of Machine Learning Research*, 18(177):1–86, 2018.

[5] Emmanuel Candès and Benjamin Recht. Exact matrix completion via convex optimization. *Commun. ACM*, 55(6):111–119, 2012.

[6] Iain M. Johnstone. On the distribution of the largest eigenvalue in principal components analysis. *The Annals of Statistics*, 29(2):295 – 327, 2001.

[7] Jinho Baik, Gérard Ben Arous, and Sandrine Péché. Phase transition of the largest eigenvalue for nonnull complex sample covariance matrices. *Annals of Probability*, 33(5):1643–1697, 2005.

[8] Peter J. Forrester. Rank 1 perturbations in random matrix theory — a review of exact results. *Random Matrices: Theory and Applications*, 12(04):2330001, 2023.

[9] Sandrine Péché. The largest eigenvalue of small rank perturbations of Hermitian random matrices. *Probability Theory and Related Fields*, 134:127–173, 2006.

[10] Mireille Capitaine, Catherine Donati-Martin, and Delphine Féral. The largest eigenvalues of finite rank deformation of large Wigner matrices: Convergence and nonuniversality of the fluctuations. *The Annals of Probability*, 37(1):1 – 47, 2009.

[11] Alex Bloemendal and Bálint Virág. Limits of spiked random matrices I. *Probability Theory and Related Fields*, 156(3–4):795–825, September 2012.

[12] That is, with an extensive number of zero entries.

[13] Simon Vary. *On low-rank plus sparse matrix sensing*. PhD thesis, University of Oxford, 2021.

[14] Marc Mézard, Giorgio Parisi, and Miguel A. Virasoro. *Spin Glass Theory and Beyond*. World Scientific, 1986.

[15] Reimer Kühn. Spectra of sparse random matrices. *Journal of Physics A: Mathematical and General*, 41(29):295002, 2008.

[16] Ginestra Bianconi. Spectral properties of complex networks. *arXiv e-prints*, page arXiv:0804.1744, April 2008.

[17] Yoshiyuki Kabashima and Hisanao Takahashi. First eigenvalue/eigenvector in sparse random symmetric matrices: influences of degree fluctuation. *Journal of Physics A: Mathematical and Theoretical*, 45(32):325001, 2012.

[18] Hisanao Takahashi. Fat-tailed distribution derived from the first eigenvector of a symmetric random sparse matrix. *Journal of Physics A: Mathematical and Theoretical*, 47(6):065003, 2014.

[19] Vito A. R. Susca, Pierpaolo Vivo, and Reimer Kühn. Top eigenpair statistics for weighted sparse graphs. *Journal of Physics A: Mathematical and Theoretical*, 52(48):485002, 2019.

[20] Vito A. R. Susca, Pierpaolo Vivo, and Reimer Kühn. Second largest eigenpair statistics for sparse graphs. *Journal of Physics A: Mathematical and Theoretical*, 54(1):015004, 2020.

[21] Barak Budnick, Preben Forer, Pierpaolo Vivo, Sabrina Aufiero, Silvia Bartolucci, and Fabio Caccioli. Top eigenpair statistics of diluted Wishart matrices. *Journal of Physics A: Mathematical and Theoretical*, 58(32):325001, 2025.

[22] Marc Mézard and Giorgio Parisi. The Bethe lattice spin glass revisited. *The European Physical Journal B*, 20:217–233, 2000.

[23] Michel Chertkov, Lukáš Kroc, Florent Krzakala, M. Vergassola, and Lenka Zdeborová. Inference in particle tracking experiments by passing messages between images. *Proceedings of the National Academy of Sciences*, 107(17):7663–7668, 2010.

[24] Guilhem Semerjian, Gabriele Sicuro, and Lenka Zdeborová. Recovery thresholds in the sparse planted matching problem. *Phys. Rev. E*, 102:022304, 2020.

[25] Yana Volkovich, Nelly Litvak, and Debora Donato. Determining factors behind the PageRank log-log plot. In *Proceedings of the 5th International Conference on Algorithms and Models for the Web-Graph*, WAW’07, page 108–123, Berlin, Heidelberg, 2007. Springer-Verlag.

[26] Predrag R. Jelenkovic and Mariana Olvera-Cravioto. Information ranking and power laws on trees. *Advances in Applied Probability*, 42:1057 – 1093, 2009.

[27] Ningyuan Chen, Nelli Litvak, and Mariana Olvera-Cravioto. Generalized pagerank on directed configuration networks. *Random Structures and Algorithms*, 51(2):237–274, 2017.

[28] Nicolas Fraiman, Tzu-Chi Lin, and Mariana Olvera-Cravioto. Stochastic recursions on directed random graphs. *Stochastic Processes and their Applications*, 166:104055, 2023.

[29] Silvia Bartolucci, Fabio Caccioli, Francesco Caravelli, and Pierpaolo Vivo. Distribution of centrality measures on undirected random networks via the cavity method. *Proceedings of the National Academy of Science (USA)*, 121(40), 2024.

[30] Charles Bordenave and Marc Lelarge. Resolvent of large random graphs. *Random Structures and Algorithms*, 37, 2010.

[31] František Slanina. Equivalence of replica and cavity methods for computing spectra of sparse random matrices. *Phys. Rev. E*, 83:011118, 2011.

[32] Jean Barbier, Mohamad Dia, Nicolas Macris, Florent Krzakala, Thibault Lesieur, and Lenka Zdeborová. Mutual information for symmetric rank-one matrix estimation: A proof of the replica formula. In *Proceedings of the 30th International Conference on Neural Information Processing Systems*, NIPS’16, page 424–432, Red Hook, NY, USA, 2016. Curran Associates Inc.

[33] Thibault Lesieur, Florent Krzakala, and Lenka Zdeborová. Constrained low-rank matrix estimation: phase transitions, approximate message passing and applications. *Journal of Statistical Mechanics: Theory and Experiment*, 2017(7):073403, 2017.

[34] Marc Lelarge and Léo Miolane. Fundamental limits of symmetric low-rank matrix estimation. In Satyen Kale and Ohad Shamir, editors, *Proceedings of the 2017 Conference on Learning Theory*, volume 65 of *Proceedings of Machine Learning Research*, pages 1297–1301. PMLR, 2017.

[35] Andrea Montanari and Alexander Wein. Equivalence of approximate message passing and low-degree polynomials in rank-one matrix estimation. *Probability Theory and Related Fields*, 191:181–233, 2024.

[36] Florent Benaych-Georges and Raj Rao Nadakuditi. The eigenvalues and eigenvectors of finite, low rank perturbations of large random matrices. *Advances in Mathematics*, 227(1):494–521, 2011.

[37] Giulio Biroli and Alice Guionnet. Large deviations for the largest eigenvalues and eigenvectors of spiked Gaussian random matrices. *Electronic Communications in Probability*, 25(70):1–13, 2020.

[38] John Wright, Arvind Ganesh, Shankar Rao, Yigang Peng, and Yi Ma. Robust principal component analysis: Exact recovery of corrupted low-rank matrices via convex optimization. In Y. Bengio, D. Schuurmans, J. Lafferty, C. Williams, and A. Culotta, editors, *Advances in Neural Information Processing Systems*, volume 22. Curran Associates, Inc., 2009.

[39] Venkat Chandrasekaran, Sujay Sanghavi, Pablo A. Parrilo, and Alan S. Willsky. Sparse and low-rank matrix decompositions. *IFAC Proceedings Volumes*, 42(10):1493–1498, 2009. 15th IFAC Symposium on System Identification.

[40] Zhouchen Lin, Risheng Liu, and Zhixun Su. Linearized alternating direction method with adaptive penalty for low-rank representation. In J. Shawe-Taylor, R. Zemel, P. Bartlett, F. Pereira, and K.Q. Weinberger, editors, *Advances in Neural Information Processing Systems*, volume 24. Curran Associates, Inc., 2011.

[41] Andrew Waters, Aswin Sankaranarayanan, and Richard Baraniuk. Sparses: Recovering low-rank and sparse matrices from compressive measurements. In J. Shawe-Taylor, R. Zemel, P. Bartlett, F. Pereira, and K.Q. Weinberger, editors, *Advances in Neural Information Processing Systems*, volume 24. Curran Associates, Inc., 2011.

[42] Praneeth Netrapalli, U N Niranjan, Sujay Sanghavi, Animashree Anandkumar, and Prateek Jain. Non-convex robust pca. In Z. Ghahramani, M. Welling, C. Cortes, N. Lawrence, and K.Q. Weinberger, editors, *Advances in Neural Information Processing Systems*, volume 27. Curran Associates, Inc., 2014.

[43] Lingyu He, Yanrong Yang, and Bo Zhang. Robust PCA for high-dimensional data based on characteristic transformation. *Australian and New Zealand Journal of Statistics*, 65(2):127–151, 2023.

[44] Thibault Lesieur, Florent Krzakala, and Lenka Zdeborová. Mmse of probabilistic low-rank matrix estimation: Universality with respect to the output channel. In *2015 53rd Annual Allerton Conference on Communication, Control, and Computing (Allerton)*, page 680–687. IEEE Press, 2015.

[45] Alice Guionnet, Justin Ko, Florent Krzakala, and Lenka Zdeborová. Low-rank matrix estimation with inhomogeneous noise. *Information and Inference: A Journal of the IMA*, 14(2), 2025.

[46] Diego Alberici, Francesco Camilli, Pierluigi Contucci, and Emanuele Mingione. The multi-species mean-field spin-glass on the nishimori line. *Journal of Statistical Physics*, 182(1), 2021.

[47] Diego Alberici, Francesco Camilli, Pierluigi Contucci, and Emanuele Mingione. A statistical physics approach to a multi-channel wigner spiked model. *Europhysics Letters*, 136(4):48001, 2022.

[48] Joshua K. Behne and Galen Reeves. Fundamental limits for rank-one matrix estimation with groupwise heteroskedasticity. In Gustau Camps-Valls, Francisco J. R. Ruiz, and Isabel Valera, editors, *Proceedings of The 25th International Conference on Artificial Intelligence and Statistics*, volume 151 of *Proceedings of Machine Learning Research*, pages 8650–8672. PMLR, 2022.

[49] Pierre Mergny, Justin Ko, and Florent Krzakala. Spectral phase transition and optimal PCA in block-structured spiked models. In Ruslan Salakhutdinov, Zico Kolter, Katherine Heller, Adrian Weller, Nuria Oliver, Jonathan Scarlett, and Felix Berkenkamp, editors, *Proceedings of the 41st International Conference on Machine Learning*, volume 235 of *Proceedings of Machine Learning Research*, pages 35470–35491. PMLR, 2024.

[50] Pierre Mergny, Justin Ko, Florent Krzakala, and Lenka Zdeborová. Fundamental limits of non-linear low-rank matrix estimation. In Shipra Agrawal and Aaron Roth, editors, *Proceedings of Thirty Seventh Conference on Learning Theory*, volume 247 of *Proceedings of Machine Learning Research*, pages 3873–3873. PMLR, 2024.

[51] Jean Barbier, Tianqi Hou, Marco Mondelli, and Manuel Sáenz. The price of ignorance: how much does it cost to forget noise structure in low-rank matrix estimation? In *Proceedings of the 36th International Conference on Neural Information Processing Systems*, NIPS ’22, Red Hook, NY, USA, 2022. Curran Associates Inc.

[52] Jean Barbier, Francesco Camilli, Marco Mondelli, and Manuel Sáenz. Fundamental limits in structured principal component analysis and how to reach them. *Proceedings of the National Academy of Sciences*, 120(30):e2302028120, 2023.

[53] Jean Barbier, Francesco Camilli, Yizhou Xu, and Marco Mondelli. Information limits and Thouless-Anderson-Palmer equations for spiked matrix models with structured noise. *Phys. Rev. Res.*, 7:013081, 2025.

[54] Florent Krzakala, Christopher Moore, Elchanan Mossel, Joe Neeman, Allan Sly, Lenka Zdeborová, and Pan Zhang. Spectral redemption in clustering sparse networks. *Proceedings of the National Academy of Science*, 110(52):20935–20940, 2013.

[55] Ki-ichiro Hashimoto. Zeta functions of finite graphs and representations of p-adic groups. In K. Hashimoto and Y. Namikawa, editors, *Automorphic Forms and Geometry of Arithmetic Varieties*, volume 15 of *Advanced Studies in Pure Mathematics*, pages 211–280. Academic Press, 1989.

[56] Alaa Saade, Florent Krzakala, and Lenka Zdeborová. Spectral density of the non-backtracking operator on random graphs. *EPL (Europhysics Letters)*, 107(5):50005, 2014.

[57] Charles Bordenave, Marc Lelarge, and Laurent Massoulié. Non-backtracking spectrum of random graphs: Community detection and non-regular Ramanujan graphs. In *Proceedings of the 2015 IEEE 56th Annual Symposium on Foundations of Computer Science (FOCS)*, FOCS ’15, page 1347–1357, USA, 2015. IEEE Computer Society.

[58] Aurelien Decelle, Florent Krzakala, Christopher Moore, and Lenka Zdeborová. Asymptotic analysis of the stochastic block model for modular networks and its algorithmic applications. *Phys. Rev. E*, 84:066106, 2011.

[59] Diego Tapias, Benedikt Grüger, Reimer Kühn, and Peter Sollich. Localization and top eigenvalue detection. *arXiv e-prints*, page arXiv:2507.07310, July 2025.

[60] Philip W. Anderson. Absence of diffusion in certain random lattices. *Phys. Rev.*, 109:1492–1505, 1958.

[61] Fernando Lucas Metz, Izaak Neri, and Désiré Bollé. Localization transition in symmetric random matrices. *Phys. Rev. E*, 82:031135, 2010.

[62] Fernando Lucas Metz and Izaak Neri. Localization and universality of eigenvectors in directed random graphs.

*Phys. Rev. Lett.*, 126:040604, 2021.

[63] Izaak Neri and Fernando Lucas Metz. Spectra of sparse non-hermitian random matrices: An analytical solution. *Phys. Rev. Lett.*, 109:030602, Jul 2012.

[64] Fernando Lucas Metz, Izaak Neri, and Tim Rogers. Spectral theory of sparse non-hermitian random matrices. *Journal of Physics A: Mathematical and Theoretical*, 52(43):434003, October 2019.

[65] Andi Han, Jiaxiang Li, Wei Huang, Mingyi Hong, Akiko Takeda, Pratik Jawanpuria, and Bamdev Mishra. Sltrain: a sparse plus low-rank approach for parameter and memory efficient pretraining. In *Proceedings of the 38th International Conference on Neural Information Processing Systems*, NIPS '24, Red Hook, NY, USA, 2024. Curran Associates Inc.

[66] Edward J. Hu, Yelong Shen, Phillip Wallis, Zeyuan Allen-Zhu, Yuanzhi Li, Shean Wang, Lu Wang, and Weizhu Chen. Lora: Low-rank adaptation of large language models. In *ICLR*. OpenReview.net, 2022.

[67] Stephen Zhang and Vardan Papyan. OATS: Outlier-Aware Pruning Through Sparse and Low Rank Decomposition. *arXiv e-prints*, page arXiv:2409.13652, September 2024.

[68] Sheldon Jay Axler. *Linear Algebra Done Right*. Undergraduate Texts in Mathematics. Springer, New York, 1997.

[69] Anthonius C. C. Coolen, Alessia Annibale, and Ekaterina Roberts. *Generating random networks and graphs*. OUP, 2017.

[70] Note that this case corresponds to the sparse symmetric matrix case analysed in Ref. [19].

[71] Yoshiyuki Kabashima, Hisanao Takahashi, and Osamu Watanabe. Cavity approach to the first eigenvalue problem in a family of symmetric random sparse matrices. *Journal of Physics: Conference Series*, 233, 2010.

[72] Vito A. R. Susca, Pierpaolo Vivo, and Reimer Kühn. Cavity and replica methods for the spectral density of sparse symmetric random matrices. *SciPost Physics Lecture Notes*, (33), 2021.

[73] Taro Nagao and Toshiyuki Tanaka. Spectral density of sparse sample covariance matrices. *Journal of Physics A: Mathematical and Theoretical*, 40(19):4973, 2007.

[74] A stronger rotationally invariant assumption (where dependence on  $\mathbf{v}$  would only be through its modulus) was shown to lead to correct solutions for harmonically coupled systems [75] and spectra of sparse random matrices [15], but was found to be too restrictive for the top eigenpair problem of the same matrix models [20, 72, 73].

[75] Reimer Kühn, Jort van Mourik, Martin Weigt, and Anette Zippelius. Finitely coordinated models for low-temperature phases of amorphous systems. *Journal Of Physics A-Mathematical And Theoretical*, 40(31):9227 – 9252, 2007.

[76] Observe that the appearance of the terms  $I_1[\pi]$  and  $I_2[\pi]$  are consistent with the derivation in [19] for a related model.

[77] Harry Kesten. Symmetric random walks on groups. *Transactions of the American Mathematical Society*, 92(2):336–354, 1959.

[78] Brendan D. McKay. The expected eigenvalue distribution of a large regular graph. *Linear Algebra and its Applications*, 40:203–216, 1981.

[79] Andries E. Brouwer and Willem H. Haemers. *Spectra of graphs*. Universitext. Springer, Germany, 2012.